Self-Interference Cancellation and Channel Estimation in Multicarrier-Division Duplex Systems With Hybrid Beamforming

BOHAN LI[1], **(Member, IEEE), LIE-LIANG YANG**[1], **(Fellow, IEEE),**
ROBERT G. MAUNDER[1], **(Senior Member, IEEE), AND**
SONGLIN SUN[2], **(Senior Member, IEEE)**

[1]School of Electronics and Computer Science, University of Southampton, Southampton SO17 1BJ, U.K.
[2]School of Information and Communication Engineering, Beijing University of Posts and Telecommunications, Beijing 100876, China

Corresponding author: Lie-Liang Yang (lly@ecs.soton.ac.uk)

ABSTRACT Design of full-duplex (FD) wireless systems faces many challenges, including self-interference cancellation (SIC), capability to provide high capacity, high flexibility for operation, best usage of resources, etc. In this paper, we propose and investigate a multicarrier-division duplex (MDD) based hybrid beamforming system operated in FD mode, which is endowed with the advantages of both time-division duplex and frequency-division duplex. It also shares some merits of FD and allows to be free of self-interference (SI) in digital domain, but faces the same challenge of SI as the FD in analog domain. Hence in this paper, we first propose an adaptive beamforming assisted SI cancellation scheme with taking into account the practical requirement of analog-to-digital conversion (ADC). It can be shown that the proposed approach is capable of jointly coping with the desired signals' transmission and SI suppression. Then, channel estimation (CEst) in MDD/MU-MIMO system is proposed by exploiting the reciprocity between the uplink and downlink subcarrier channels that is provided by MDD. Correspondingly, the orthogonality-achieving pilot symbols are designed, and the least-square (LS) CEst as well as linear minimum mean-square error (LMMSE) CEst are derived. Finally, the performance of MDD/MU-MIMO systems employing the proposed SIC method is investigated, with respect to the SI cancellation capability, sum-rate potential, CEst performance, and the effect of CEst on the achievable performance. Our studies show that MDD/MU-MIMO provides an effective option for design of future wireless transceivers.

INDEX TERMS Full-duplex, multicarrier-division duplex, self-interference cancellation, hybrid beamforming, channel estimation, least square, linear minimum mean square error.

I. INTRODUCTION

Achieving the highest possible spectral efficiency to meet the demand of ever increasing data rate has always been a top priority in the design of wireless communication systems, especially, of the fifth-generation (5G) (and beyond) wireless systems [1], [2]. Currently, all wireless networks are operated in half-duplex (HD) mode, based on either time-division duplex (TDD) or frequency-division duplex (FDD). Specifically in cellular wireless systems, downlink (DL)

The associate editor coordinating the review of this manuscript and approving it for publication was Wenchi Cheng.

and uplink (UL) transmissions are supported by different time-slots or different frequency bands. However, these HD modes have some weakness in terms of system performance and complexity, hindering them from employment in future wireless systems. For instance, although FDD enables DL and UL transmissions at the same time and avoids interference between DL and UL, the complexity and overhead for channel estimation (CEst) in large-scale antenna systems may be unaffordable, due to the incoherence of UL/DL channels. On the other hand, TDD can benefit from the reciprocity between DL and UL channels, making it possible that only base station (BS) needs to estimate the UL channels, while the

IEEE Access·

B. Li *et al.*: Self-Interference Cancellation and Channel Estimation in Multicarrier-Division Duplex Systems With Hybrid Beamforming

DL channel state information (CSI) can be derived from the UL CEst. However, in TDD-based systems, guard time between DL/UL switching is required, which may be significant in future broadband wireless systems, yielding serious delay and inefficient usage of resources [3].

Due to the limitation of TDD and FDD, full duplex (FD), more specifically in-band full duplex (IBFD), has received increasing interest in recent years, owing to its potential to nearly double the capacity of a wireless channel [4]–[6]. However, to make IBFD systems feasible, it is critical to efficiently suppress the self-interference (SI) generated by a node's transmitted signal on its own received signal, which is usually significant in real wireless systems. According to [4], for a IBFD-based BS to achieve a link signal-to-noise ratio (SNR) equating to that of a HD counterpart, it is typically required to suppress SI by about 110 dB. To achieve this target, various SI cancellation (SIC) techniques, operated in propagation-, analog- or/and digital-domain, have been proposed and investigated in literature, as seen, for example, in the papers [4]–[9].

On the other hand, the heterogeneous wireless systems in 5G and beyond will in no doubt rely on multicarrier signaling, in the principles of orthogonal frequency division multiplexing (OFDM) and non-orthogonal multiple access (NOMA). Owing to this consideration, an out-band FD (OBFD) scheme, referred to as multicarrier division duplex (MDD), has been proposed in [10] and further studied in [11], [12]. The studies of [12] show that MDD is capable of exploiting the advantages of both FDD and TDD, and employs the potential to outperform both the HD and IBFD schemes in some application scenarios. To be more specific, MDD may be deemed to be a frequency-domain counterpart of TDD and hence, employs all the advantages of TDD. For example, instead of a flexible UL/DL time-slot allocation, MDD can rely on the flexible UL/DL subcarrier allocation to attain the reciprocity between UL and DL. Like TDD, MDD is also flexible to support asymmetrical UL/DL traffics by assigning the corresponding number of subcarriers to UL/DL. However, MDD may outperform TDD by saving the guard-time required by the TDD for UL/DL switching. MDD can also inherit the merits of FDD. For example, under FDD, there is no switch-over between the transmission and receiving of a node on a same frequency. Similarly in MDD, there is also no switch-over of this kind, provided that the subcarriers assigned to a node for receiving and transmission are not changed. MDD also outperform FDD in terms of CEst, as MDD is capable of exploiting the reciprocity between UL and DL for CEst, while the UL/DL channels in FDD are not reciprocal. In other words, relying on MDD, the CSI required for DL transmitter preprocessing can be obtained from the CSI estimated from the UL receiving, with the aid of the frequency-domain correlation of wireless channels. Furthermore, since in MDD systems, UL channel training and DL transmission happen concurrently, MDD mode can substantially mitigate the channel aging problem that TDD/FDD

modes experience, when channel's time-varying becomes relatively fast [13].

In comparison with the IBFD schemes [4], [5], where transmission and receiving happen at the same time and on the same frequency (subcarrier), MDD allows transmission and receiving to use the same time and frequency resources but different subcarriers. This arrangement allows to relax the SIC requirement of IBFD, and achieve the SI-free signal processing in digital-domain. Nevertheless, MDD is a type of FD, it succeeds the challenges of general FD systems, such as the effect of SI on receiver's ADC. However, MDD has its advantage that SI may be near-perfectly removed in the digital domain, provided that the SI is sufficiently suppressed in the propagation/analog domains, so that the received signals (SI plus desired signal) fall within the dynamic range of receiver's ADC. In other words, once SI is sufficiently suppressed in propagation/analog domains so that the total received signals can be operated within the ADC's dynamic range, the FFT operation in receiver is able to help to remove all the residual SI without any extra complexity. Therefore, in MDD-based systems, SIC is only required in the propagation and analog domains.

Owing to the merits of MDD as above-mentioned, in this paper, we investigate the efficient SIC methods for the MDD-based multiuser multiple-input multiple-output (MDD/MU-MIMO) system, as well as its channel estimation by leveraging the correlation existing between DL and UL subcarriers.

A. RELATED WORKS

From literature [14]–[19] we know that in the context of the conventional FD MIMO systems, various SIC methods in the propagation and analog domains have been proposed. These SIC methods may also be introduced to the MDD/MU-MIMO systems. However, when MDD/MU-MIMO system is in the large-scale, explained by the number of transmit/receive antennas, the traditional SIC approaches for MIMO may not be suitable, due to the consequence of huge overhead and complexity. Fortunately, in this case, the big number of antennas can be leveraged for SI suppression. To this end, beamforming based SIC has become one of the most important methods for SI reduction. Specifically in [20], a full-digital precoder has been designed to point SI signals to the null space of desired received signals and, thereby, cancel the SI signals in analog domain. By properly designing the full-digital precoders, SI can also be suppressed along with the maximization of sum-rate [21], [22]. Instead of full-digital precoding, as shown in [23], hybrid precoding is capable of achieving the SI reduction of upto 30 dB. However, to the best of our knowledge, on the joint design of desired signal transmission and SIC, all the beamforming based SIC methods presented so far only provide a fixed amount of SI reduction. This may not satisfy the different requirements of analog-domain SI reduction in practice and, consequently, causes large quantization noise after ADC, if SI

B. Li *et al.*: Self-Interference Cancellation and Channel Estimation in Multicarrier-Division Duplex Systems With Hybrid Beamforming

IEEE *Access*

TABLE 1. Comparison of beamforming based SIC methods.

	System model	Operation mode	SIC method	Feature
This paper	Large-scale MU-MIMO	MDD (OBFD)	Hybrid beamforming SIC; Digital-domain SIC by FFT operation	SIC requirement modeling of ADC; Provide SI reduction upto 300 dB; Joint design of desired transmission and SIC
[9], [20]	MU-MIMO	IBFD	Full-digital beamforming SIC	Different antenna array deployments
[21]	Point-to-point MIMO	IBFD	Full-digital beamforming SIC	Joint design of desired transmission and SIC
[22]	MU-MIMO	IBFD	Full-digital beamforming SIC	Joint design of desired transmission and SIC
[23]	Point-to-point MIMO	IBFD	Hybrid beamforming SIC	Provide SI reduction upto 30 dB
[12]	Point-to-point MIMO	MDD (OBFD)	Full-digital beamforming SIC; Digital-domain SIC by FFT operation	Consideration of ADC requirement

reduction is insufficient. Furthermore, in these references, only the point-to-point single-carrier MIMO communication scenarios have been considered. Additionally, in [12], the MDD-assisted point-to-point multicarrier MIMO system employing full-digital precoder/combiner has been proposed and studied, demonstrating that MDD-mode is capable of outperforming HD and IBFD modes in some communication scenarios. However, when antenna arrays become large, the full-digital SIC methods are no longer feasible in hybrid beamforming systems. Hence, to satisfy the requirement of ADC in various communication environments, the study on the dynamic SI reduction in the hybrid beamforming assisted IBFD or OBFD systems is highly important, but has not been considered in open literature.

B. CONTRIBUTIONS

Against the background, in this paper, we study the MDD/MU-MIMO hybrid beamforming systems associated with the following issues. *Firstly*, the SIC requirement for ADC to efficiently operate in its dynamic range is modeled. Then, to make MDD-mode feasible in large-scale MU-MIMO systems, we propose an adaptive beamforming based SIC method via analog precoder/combiner design in order to dynamically suppress SI, which has not been investigated in the open literature. Various design options are addressed by taking account of the trade-off between performance and complexity. Furthermore, zero-forcing (ZF) and minimum mean squared error (MMSE) algorithms are respectively introduced to design the digital precoder and combiner. Our studies show that the proposed beamforming SIC method are capable of simultaneously suppressing the SI while maintaining the performance of desired DL/UL communications, when appropriate initialization is applied in the proposed algorithms. Furthermore, our proposed method is capable of providing SIC over a big dynamic range upto 300 dB, which is achieved via applying different system configurations and an appropriate number of SIC iterations.

Secondly, we address the CEst in MDD/MU-MIMO systems, and consider the estimation of both UL and DL channels by exploiting the correlation existing among subcarriers and the reciprocity existing between the UL and DL channels. To be more specific, we first design a set of frequency-domain orthogonality-achieving pilot symbols (PSs) for estimating the UL/DL channels of all mobile stations (MSs). Based

on these orthogonality-achieving PSs, the least square (LS) CEst is implemented to obtain the time-domain UL channel impulse response (CIR), from which the UL/DL CIRs of all subcarriers are derived with the aid of the above-mentioned subcarrier correlation and reciprocity of UL/DL channels. Furthermore, we consider the CEst in the scenario where employing orthogonality-achieving PSs is impossible due to a big number of MSs and/or randomly distributed UL subcarriers. Correspondingly, the CEst is accomplished in the principles of linear minimum mean square error (LMMSE).

Finally, we investigate and compare the performance of the MDD/MU-MIMO systems. First, we demonstrate the performance of the proposed SIC schemes. Then, the spectral-efficiency performance of MDD/MU-MIMO systems with various beamforming aided SIC options is investigated and compared. Furthermore, the performance of the proposed CEst schemes is demonstrated, and the impact of CEst on the achievable spectral-efficiency is studied and compared. Our studies show that the LS CEst relying on the orthogonality-achieving PSs enables the MDD/MU-MIMO system to achieve nearly the same sum-rate as the counterpart system with perfect CSI. In the case that orthogonality-achieving PSs are impossible, the LMMSE CEst is promising, allowing to achieve the sum-rate close to that attained under the assumption of perfect CSI.

The novelty of our work is compared with the related works in Table 1. Note that in addition to the differences stated in the table, the channel estimation in MDD-based systems was not considered in [12]. The contributions of this paper can be summarized as follows:

- As both IBFD and OBFD have to implement efficient SIC to make the FD-relied operations feasible, an adaptive beamforming based SIC scheme is proposed to achieve the ADC's requirement for SI reduction. The proposed SIC scheme is capable of providing a big range of SIC in analog domain while at only little cost of system performance. We also demonstrate the impact of the Rician factor of SI channel, the number of antennas and the angle between TX/RX antenna arrays on the performance of SIC, from which we can gain insight for the system configuration of not only the MDD-based systems but also other IBFD systems.

- Hybrid precoding and combining schemes with SIC capability are designed for MDD/MU-MIMO systems.

IEEE *Access*

B. Li *et al.*: Self-Interference Cancellation and Channel Estimation in Multicarrier-Division Duplex Systems With Hybrid Beamforming

The studies and performance results, including the robustness of proposed SIC scheme and the performance of MDD/MU-MIMO systems, convince us the effectiveness of the designed schemes and also the merits of MDD-relied systems.

- By leveraging subcarrier correlation and reciprocity between UL and DL channels, an efficient CEst method is presented for obtaining the CSI of both UL and DL channels. Specific subcarrier allocation for frequency-domain pilot transmission is proposed to benefit CEst. Furthermore, to reduce system overhead in more general scenarios, a CEst method based on LMMSE is presented and studied, which is also capable of allowing MDD/MU-MIMO systems to achieve promising performance.

The rest of the paper is organized as follows. In Section II, we address the modeling in MDD/MU-MIMO systems, including transmitter, channel and receiver models, as well as the modeling of ADC. In Section III, the hybrid beamforming is designed with the objective to maximize sum-rate while simultaneously meet the SIC target. CEst is studied in Section IV, while simulation results are demonstrated in Section V. Finally, in Section VI, we summarize the findings from research and consider their implications.

Throughout the paper, the following notations are used: $\boldsymbol{A}$, $\boldsymbol{a}$ and a are for matrix, vector, and scalar, respectively; $\mathcal{A}$ represents set; $\boldsymbol{a}(i)$ denotes the i-th element of $\boldsymbol{a}$, and $\boldsymbol{A}(i,j)$ denotes the (i,j)-th element of $\boldsymbol{A}$; $|\boldsymbol{A}|$, $\boldsymbol{A}^*$, $\boldsymbol{A}^T$, $\boldsymbol{A}^{-1}$ and $\boldsymbol{A}^H$ represent, respectively, the determinant, complex conjugate, transpose, inverse and Hermitian transpose of $\boldsymbol{A}$; diag$(a, b, \ldots)$ means a diagonal matrix with the diagonal entries of $(a, b, \ldots)$, diag$(\boldsymbol{a})$ means a diagonal matrix formed from $\boldsymbol{a}$, and $\boldsymbol{I}_N$ denotes a $(N \times N)$ identity matrix; $\mathcal{CN}(\boldsymbol{0}, \boldsymbol{A})$ represents the zero-mean complex Gaussian distribution with covariance matrix $\boldsymbol{A}$; Furthermore, Tr$(\cdot)$, log$(\cdot)$ and $\mathbb{E}[\cdot]$ denote the trace, logarithmic and expectation operators, respectively.

II. SYSTEM MODEL

We consider a MDD/MU-MIMO system, where a N-element transmit antenna array at BS uses N_{RF} radio-frequency (RF) chains to serve D DL mobile stations (MSs) and simultaneously, a $\bar{N}$-element receive antenna array also at BS uses $\bar{N}_{\mathrm{RF}}$ RF chains to serve $\bar{D}$ UL MSs. Hence, the total number of MSs is $D_{\mathrm{sum}} = D + \bar{D}$. All MSs are equipped with single antenna. In our proposed system, the BS works in MDD mode, while MSs are operated in HD mode. As shown in Fig. 1, we assume that the transmitter and receiver at BS are reasonably separated in space, and both of them are equipped with the uniformly spaced linear antenna array (ULA). We assume OFDM-assisted data transmission, that the channels between BS and MSs experience frequency selective fading, and that sufficient cyclic prefix (CP) is invoked to avoid inter-symbol interference (ISI). Furthermore, following the principles of MDD [12], subcarriers are
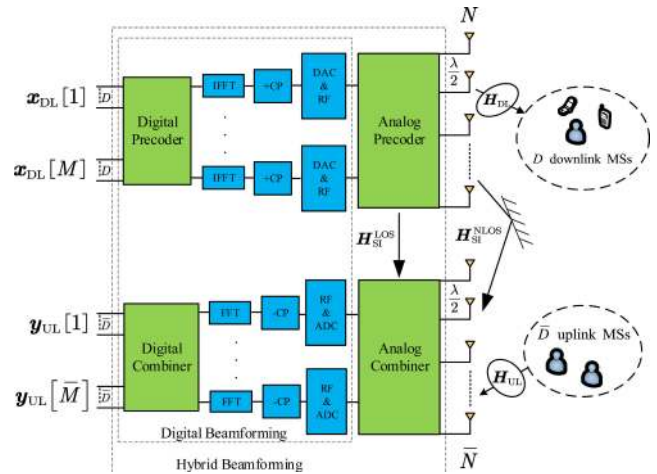

FIGURE 1. Schematic diagram of the MDD/MU-MIMO system.

divided into two mutually exclusive subsets, namely a DL subcarrier subset $\mathcal{M}$ with M subcarriers, and an UL subcarrier subset $\bar{\mathcal{M}}$ with $\bar{M}$ subcarriers, i.e., $|\mathcal{M}| = M$ and $|\bar{\mathcal{M}}| = \bar{M}$. The total number of subcarriers is expressed as $M_{\mathrm{sum}} = M + \bar{M}$. We assume that UL/DL MSs are scheduled in such a way, so that the interference generated by UL MSs on a DL MS is sufficiently low, without distorting the operation of the DL MSs' receiver ADCs.

A. COMMUNICATIONS CHANNEL MODEL

The channel between the n-th transmit antenna at BS and the d-th DL MS is modeled by a L-tap frequency-selective fading channel, with the time-domain CIR (TDCIR) expressed as [24]

$$\boldsymbol{g}_{n,d}^{\mathrm{DL}} = \left[g_{n,d}[1], \ldots, g_{n,d}[l], \ldots, g_{n,d}[L] \right]^T \quad (1)$$

where $g_{n,d}^{\mathrm{DL}}[l] = \alpha_{n,d,l}^{\mathrm{DL}}$ follows a complex Gaussian distribution of $\alpha_{n,d,l}^{\mathrm{DL}} \sim \mathcal{CN}(0, 1/L)$. Similarly, the UL channel between the $\bar{d}$-th UL MS and the $\bar{n}$-th receive antenna at BS is defined as the L-tap TDCIR expressed as $\boldsymbol{g}_{\bar{n},\bar{d}}^{\mathrm{UL}}$. Furthermore, when the same frequency band is considered, which is the case in MDD mode, we have $\boldsymbol{g}_{n,d}^{\mathrm{DL}} = \boldsymbol{g}_{n,d}^{\mathrm{UL}}$, meaning that there is no distinction between UL and DL channels, i.e., they are reciprocal. Hence, when there is no confusion, the notations 'DL' and 'UL' are removed.

According to the principles of OFDM [10], the frequency-domain CIR (FDCIR) $\boldsymbol{h}_{n,d}$ can be obtained as

$$\boldsymbol{h}_{n,d} = \boldsymbol{F} \boldsymbol{\Psi} \boldsymbol{g}_{n,d} \quad (2)$$

where $\boldsymbol{F} \in \mathbb{C}^{M_{\mathrm{sum}} \times M_{\mathrm{sum}}}$ is the FFT matrix, $\boldsymbol{\Psi} \in \mathbb{C}^{M_{\mathrm{sum}} \times L}$ is constructed by the first L columns of $\boldsymbol{I}_{M_{\mathrm{sum}}}$. Furthermore, the DL subchannels $\boldsymbol{h}_{n,d}^{\mathrm{DL}}$ and UL subchannels $\boldsymbol{h}_{n,d}^{\mathrm{UL}}$ between the n-th antenna at BS and the d-th MS can be obtained from (2), which can be expressed as

$$\boldsymbol{h}_{n,d}^{\mathrm{DL}} = \boldsymbol{\Phi}_{\mathrm{DL}}^T \boldsymbol{h}_{n,d} = \left[h_{n,d}[1], \ldots, h_{n,d}[m], \ldots, h_{n,d}[M] \right]^T$$

$$(3)$$

B. Li et al.: Self-Interference Cancellation and Channel Estimation in Multicarrier-Division Duplex Systems With Hybrid Beamforming

IEEE Access

$$\boldsymbol{h}_{n,d}^{\text{UL}} = \boldsymbol{\Phi}_{\text{UL}}^T \boldsymbol{h}_{n,d} = [h_{n,d}[1], \ldots, h_{n,d}[\bar{m}], \ldots, h_{n,d}[\bar{M}]]^T \tag{4}$$

where $\boldsymbol{\Phi}_{\text{DL}}^T \in \mathbb{C}^{M \times M_{\text{sum}}}$ and $\boldsymbol{\Phi}_{\text{UL}}^T \in \mathbb{C}^{\bar{M} \times M_{\text{sum}}}$ are the mapping matrices, constructed from $\boldsymbol{I}_{M_{\text{sum}}}$ by choosing the columns corresponding to the particular subcarriers assigned to DL and UL, respectively.

B. SELF-INTERFERENCE CHANNEL MODEL

Since both UL and DL are operated in the same frequency band based on MDD, the MDD/MU-MIMO system experiences self-interference (SI), as shown in Fig.1. We assume that the SI channel experiences Rician fading, constituting both line-of-sight (LOS) component and non-line-of-sight (NLOS) component, which is expressed as [23]

$$\boldsymbol{H}_{\text{SI}} = \sqrt{\frac{\kappa}{\kappa+1}} \boldsymbol{H}_{\text{SI}}^{\text{LOS}} + \sqrt{\frac{1}{\kappa+1}} \boldsymbol{H}_{\text{SI}}^{\text{NLOS}} \tag{5}$$

where κ is the Rician factor. As the transmit and receiver antennas at BS are close to each other, $\boldsymbol{H}_{\text{SI}}^{\text{LOS}}$ denotes the LOS near-field flat fading channel, with the (i, j)-th element expressed as [25]

$$\boldsymbol{H}_{\text{SI}}^{\text{LOS}}(i, j) = \frac{\rho}{r_{ij}} \exp\left(-j2\pi \frac{r_{ij}}{\lambda}\right) \tag{6}$$

where ρ is the power normalization constant making $\mathbb{E}[||\boldsymbol{H}_{\text{SI}}^{\text{LOS}}||_F^2] = N\bar{N}$, r_{ij} is the distance between the i-th element of transmit array and the j-th element of receive array, and λ is the wavelength. By contrast, $\boldsymbol{H}_{\text{SI}}^{\text{NLOS}}$ in (5) denotes the NLOS channel, which is assumed to follow the flat Rayleigh fading, with its elements obeying the distribution of $\boldsymbol{H}_{\text{SI}}^{\text{NLOS}}(i, j) \sim \mathcal{CN}(0, 1)$.

C. REQUIREMENT OF SELF-INTERFERENCE CANCELLATION

In full-duplex systems, ADC is the most critical component determining the system operability and achievable performance. A practical ADC has only limited dynamic range and resolution. Hence, if the input signal to an ADC is beyond a particular level, the signal will be distorted, yielding large quantization noise and non-linear distortion, which would further decrease the performance of the following digital-domain signal processing [26]. Specifically, when assuming a Q-bit ADC, the signal to quantization noise ratio (SQNR) is about $6.02Q$ [27]. When given the bandwidth of B (Hz), the noise floor at receiver is given by [5] $-174 + k_N + 10\log(B)$ dBm, where k_N is noise factor. Hence, the maximum input signal power to the receiver is

$$s_{\max}(dBm) = -174 + k_N + 10\log(B) + 6.02Q \tag{7}$$

Therefore, for a SI contaminated signal to pass an ADC without distortion, the propagation- and analog-domain SI cancellation should provide the SIC of at least [26]

$$C_{\text{SI}}^{\text{Demand}}(dB) = P_{\text{DL}}(dBm) - s_{\max}(dBm) + 10(dB) \tag{8}$$

where P_{DL} is the transmit power of DL, while 10 dB is added to account for the PAPR, as an OFDM signal's power may rise upto 10 dB above the average power [28].

After the propagation- and analog-domain SIC, the SI input to ADC of BS receiver is $P_{\text{SI}} = P_{\text{DL}} - C_{\text{SI}}$, where C_{SI} is the total SI reduced in the propagation- and analog-domains. Hence with the aid of (8), we know that when given P_{DL}, the SIC should satisfy the SIC requirement of

$$\frac{P_{\text{DL}}}{P_{\text{SI}}} \geq 10^{\frac{C_{\text{SI}}^{\text{Demand}}}{10}} \tag{9}$$

Above we have provided the channel models in the MDD/MU-MIMO systems, and analyzed the target for SI cancellation. Below we start considering the transceiver design for the MDD/MU-MIMO systems.

D. TRANSMITTER MODEL

For DL transmission, let the symbol vector transmitted by BS on the DL subcarriers be expressed as $\boldsymbol{x}_{\text{DL}}[m] \in \mathbb{C}^{D \times 1}$, which is normalized to satisfy $\mathbb{E}\left[\boldsymbol{x}_{\text{DL}}[m]\boldsymbol{x}_{\text{DL}}[m]^H\right] = \boldsymbol{I}_D$. In order to mitigate SI and attain beamforming gain, at transmitter, $\boldsymbol{x}[m]$ is processed by a precoder $\boldsymbol{F}[m] \in \mathbb{C}^{N \times D}$, with the constraint of $\|\boldsymbol{F}[m]\|_F^2 \leq P_m$, where P_m is the maximum transmit power of the m-th DL subcarrier. The total transmit power of DL satisfies $\sum_{m=1}^{M} P_m \leq P_{\text{DL}}$. As shown in Fig. 1, the transmitter precoder constitutes a digital precoder $\boldsymbol{F}_{\text{BB}}[m]$ for each individual DL subcarrier and an analog precoder $\boldsymbol{F}_{\text{RF}}$ that is common to all DL subcarriers. Hence, the overall precoding for a DL subcarrier can be expressed as $\boldsymbol{F}[m] = \boldsymbol{F}_{\text{RF}}\boldsymbol{F}_{\text{BB}}[m]$, where $\boldsymbol{F}_{\text{RF}} \in \mathbb{C}^{N \times N_{\text{RF}}}$, and $\boldsymbol{F}_{\text{BB}}[m] \in \mathbb{C}^{N_{\text{RF}} \times D}$. The baseband signal transmitted on the m-th subcarrier can be expressed as

$$\boldsymbol{s}_{\text{DL}}[m] = \boldsymbol{F}[m]\boldsymbol{x}_{\text{DL}}[m], \quad m = 1, 2, \ldots, M \tag{10}$$

where $\boldsymbol{s}[m] \in \mathbb{C}^{N \times 1}$.

E. RECEIVER MODEL

When given the transmitted signal as shown in (10), the received signals by the D MSs from the m-th subcarrier can be expressed as

$$\boldsymbol{y}_{\text{DL}}[m] = \boldsymbol{H}_{\text{DL}}[m]\boldsymbol{F}[m]\boldsymbol{x}_{\text{DL}}[m] + \boldsymbol{z}_{\text{DL}}[m] \tag{11}$$

where $\boldsymbol{H}_{\text{DL}}[m] \in \mathbb{C}^{D \times N}$ and $\boldsymbol{z}[m] \sim \mathcal{CN}(\boldsymbol{0}, \sigma^2 \boldsymbol{I}_D)$ are the DL channel matrix and additive Gaussian noise corresponding to the m-th DL subcarrier, respectively. It is noteworthy that for simplicity we ignore the interference from UL MSs to DL MSs in (11), so that we can focus on the SIC and channel estimation in MDD/MU-MIMO systems.[1]

On the other side, the signals transmitted at BS also propagate to its receive antenna array for the UL. This SI signal at

---

[1]Note furthermore that the interference from UL MSs to DL MSs in FD-based systems can be effectively mitigated via the scheduling at medium access control (MAC) layer [29]–[31]. However, the in-depth research in the context of MDD-based systems is required, which will be addressed in our future work.

IEEE Access

B. Li et al.: Self-Interference Cancellation and Channel Estimation in Multicarrier-Division Duplex Systems With Hybrid Beamforming

m-th subcarrier after the analog combining can be expressed as

$$y_{\mathrm{SI}}[m] = W_{\mathrm{RF}}^H H_{\mathrm{SI}} F[m] x_{\mathrm{DL}}[m] \qquad (12)$$

In (12), $W_{\mathrm{RF}} \in \mathbb{C}^{\bar{N} \times \bar{N}_{\mathrm{RF}}}$ is the analog combiner, which is regarded as the pseudo-identity matrix in digital beamforming system, i.e. $W_{\mathrm{RF}} = I_{\bar{N} \times \bar{N}_{\mathrm{RF}}}$ [32]. Based on (12), the total SI power entering the ADC in the BS receiver is given by $P_{\mathrm{SI}} = \sum_{m=1}^{M} \mathbb{E} \|y_{\mathrm{SI}}[m]\|_2^2$.

Note that the distance between the transmitter and receiver arrays at BS is much smaller than the communication links from MSs to BS, which leads to SI signals to be 50-100 dB stronger than the desired signals received from UL. This means that although DL and UL are operated on different subcarriers, prior to digitization, UL signals would be overwhelmed by SI signals in ADC, if propagation- and analog-domain SIC cannot provide sufficient SI reduction. In this case, quantization noise may be significant and unable to be mitigated by any digital-domain signal processing techniques. Therefore, a certain amount of SI reduction has to be achieved to satisfy (9) prior to the ADC at receiver. On the other side, provided that the constraint of (9) is satisfied, as shown in Fig. 1, the received digital signals after RF processing and ADC can be expressed as

$$y_{\mathrm{UL}}[\bar{m}] = W_{\mathrm{RF}}^H H_{\mathrm{UL}}[\bar{m}] x_{\mathrm{UL}}[\bar{m}]$$
$$+ \sum_{m \in \mathcal{M}} W_{\mathrm{RF}}^H H_{\mathrm{SI}} F[m] x_{\mathrm{DL}}[m] + W_{\mathrm{RF}}^H z_{\mathrm{UL}}[\bar{m}] \quad (13)$$

where $x_{\mathrm{UL}}[\bar{m}]$ denotes the UL data symbols satisfying $\mathbb{E}[\bar{x}_{\mathrm{DL}}[m] \bar{x}_{\mathrm{DL}}[m]^H] = I_{\bar{D}}$, $z_{\mathrm{UL}}[\bar{m}]$ is the complex Gaussian noise obeying the distribution of $\mathcal{CN}(0, \sigma^2 I_{\bar{N}})$. Furthermore, after CP removing and digital-domain SIC by FFT operation, the final signal for UL detection can be expressed as

$$y_{\mathrm{UL}}[\bar{m}] = W^H[\bar{m}] H_{\mathrm{UL}}[\bar{m}] x_{\mathrm{UL}}[\bar{m}] + W^H[\bar{m}] z_{\mathrm{UL}}[\bar{m}] \quad (14)$$

for $\bar{m} = 1, 2, \ldots, \bar{M}$, where $W[\bar{m}] = W_{\mathrm{RF}} W_{\mathrm{BB}}[\bar{m}]$, $W_{\mathrm{BB}}[\bar{m}] \in \mathbb{C}^{\bar{N}_{\mathrm{RF}} \times \bar{D}}$.

III. ADAPTIVE BEAMFORMING-AIDED SELF-INTERFERENCE CANCELLATION

In this section, we address the beamforming-aided SIC implemented via the design of hybrid precoder/combiner. The objective of SIC is to make the SIC requirement of (9) be satisfied.

According to (12), the power of SI signals before ADC can be evaluated as

$$P_{\mathrm{SI}} = \sum_{m=1}^{M} \mathbb{E}\left\{ \mathrm{Tr}\left(y_{\mathrm{SI}}[m]^H y_{\mathrm{SI}}[m] \right) \right\}$$
$$= \mathrm{Tr}\left(F_{\mathrm{RF}}^H H_{\mathrm{SI}}^H W_{\mathrm{RF}} W_{\mathrm{RF}}^H H_{\mathrm{SI}} F_{\mathrm{RF}} \sum_{m=1}^{M} F_{\mathrm{BB}}[m] F_{\mathrm{BB}}^H[m] \right)$$
$$(15)$$

From this equation we can know that P_{SI} is proportional to $P'_{\mathrm{SI}} = \mathrm{Tr}(F_{\mathrm{RF}}^H H_{\mathrm{SI}}^H W_{\mathrm{RF}} W_{\mathrm{RF}}^H H_{\mathrm{SI}} F_{\mathrm{RF}})$. Hence, P_{SI} can

be reduced via minimizing P'_{SI}. Therefore, according to the structure of P'_{SI}, we consider two design options for SIC, which are depended on the optimization of F_{RF} and W_{RF}, respectively, in analog domain.

A. PRECODING OPTIMIZATION AIDED SELF-INTERFERENCE CANCELLATION

The first design option assumes that SI suppression is solely depended on the design of F_{RF} at transmitter. Thereby, the design of combiner at receiver only focuses on the UL transmissions without considering the impact of SI. In this paper, we consider the MMSE method for UL combining [33], and the full-digital combiner can be expressed as [34]

$$W_{\mathrm{MMSE}}[\bar{m}] = \left(H_{\mathrm{UL}}[\bar{m}] H_{\mathrm{UL}}^H[\bar{m}] + \sigma^2 I \right)^{-1} H_{\mathrm{UL}}[\bar{m}],$$
$$\bar{m} = 1, 2, \ldots, \bar{M}. \quad (16)$$

Then, the hybrid UL combiners can be designed to approximate $W_{\mathrm{MMSE}}[\bar{m}]$, formulated as

$$\arg \min_{W_{\mathrm{RF}}; W_{\mathrm{BB}}[1], \ldots, W_{\mathrm{BB}}[\bar{M}]} \sum_{\bar{m}=1}^{\bar{M}} \| W_{\mathrm{MMSE}}[\bar{m}] - W_{\mathrm{RF}} W_{\mathrm{BB}}[\bar{m}] \|_F^2$$
$$\text{subject to } |W_{\mathrm{RF}}(i, j)| = 1, \quad \forall i, j \quad (17)$$

The optimization problem of (17) is a typical one in the design of hybrid beamforming, which can be solved by different algorithms, such as that in [35]–[39]. Specifically in the performance study in Section V of this paper, we introduce the projected gradient descent (PGD) algorithm [38], [39]. Readers interesting in the details of the algorithm are referred to these reference.

After W_{RF} is obtained, the SI suppression can be executed based on the optimization of

$$\arg \min_{F_{\mathrm{RF}}} f(F_{\mathrm{RF}}) \qquad (18a)$$
$$\text{subject to } |F_{\mathrm{RF}}(i, j)| = 1, \quad \forall i, j \qquad (18b)$$
$$\frac{P_{\mathrm{DL}}}{P_{\mathrm{SI}}} \geq 10^{\frac{C_{\mathrm{SI}}^{\mathrm{Demand}}}{10}} \qquad (18c)$$

where $f(F_{\mathrm{RF}}) = \mathrm{Tr}(H_{\mathrm{w}} F_{\mathrm{RF}} F_{\mathrm{RF}}^H H_{\mathrm{w}}^H)$ with $H_{\mathrm{w}} = W_{\mathrm{RF}}^H H_{\mathrm{SI}}$. However, this optimization problem is non-convex and hard to solve. To circumvent this dilemma and reduce the computational complexity, we propose an adaptive algorithm based on the cyclic coordinate descent (CDC) algorithm [40]–[43], so as to dynamically suppress SI. It is noteworthy that the performance of the CDC algorithm is sensitive to the initialization [44]. Hence, in order to suppress SI while simultaneously maintain the required performance of DL, the initialization of F_{RF} is very important in our algorithm. In Section V-A, we will investigate the effect of the initialization of F_{RF} on the achievable performance. Furthermore, to calculate P_{SI} during the optimization process, the digital precoder for the m-th subcarrier is assumed to be in ZF principle, which yields

$$F_{\mathrm{BB}}^{\mathrm{ZF}}[m] = H_{\mathrm{eq}}^H[m] \left(H_{\mathrm{eq}}[m] H_{\mathrm{eq}}^H[m] \right)^{-1} P^{\frac{1}{2}}[m], \quad m \in \mathcal{M} \quad (19)$$

B. Li et al.: Self-Interference Cancellation and Channel Estimation in Multicarrier-Division Duplex Systems With Hybrid Beamforming

IEEE Access

where $\boldsymbol{H}_{\mathrm{eq}}[m] = \boldsymbol{H}_{\mathrm{DL}}[m]\boldsymbol{F}_{\mathrm{RF}}$ is the resultant channel after the analog precoding, $\boldsymbol{P}[m] = \mathrm{diag}(p_1[m], p_2[m], \ldots, p_D[m])$ is obtained from the water-filling algorithm [45].

To solve the optimization problem (18) iteratively, the element $\boldsymbol{F}_{\mathrm{RF}}(i, j)$ is firstly optimized by assuming that all the other elements are fixed. In this case, (18a) can be simplified to

$$f(\boldsymbol{F}_{\mathrm{RF}}) = \mathrm{Tr}(\boldsymbol{A}_j) + \boldsymbol{f}_{\mathrm{RF}}^{(j)\,H} \boldsymbol{H}_{\mathrm{w}}^{H} \boldsymbol{H}_{\mathrm{w}} \boldsymbol{f}_{\mathrm{RF}}^{(j)}$$
$$= \mathrm{Tr}(\boldsymbol{A}_j) + \zeta_{ij}^{\tilde{H}} + 2\mathrm{Re}\{\boldsymbol{F}_{\mathrm{RF}}^{*}(i, j)\eta_{ij}^{\tilde{H}}\} \quad (20)$$

where $\zeta_{ij}^{\tilde{H}} = \tilde{\boldsymbol{H}}_j(i, i) + 2\mathrm{Re}\left\{\sum_{m\neq i,n\neq i} \boldsymbol{F}_{\mathrm{RF}}^{*}(m, j)\,\tilde{\boldsymbol{H}}_j(m, n)\right.$

$\left.\boldsymbol{F}_{\mathrm{RF}}(n, j)\right\}$, $\eta_{ij}^{\tilde{H}} = \sum_{m\neq i} \tilde{\boldsymbol{H}}_j(i, m)\boldsymbol{F}_{\mathrm{RF}}(m, j)$, associated with

$\tilde{\boldsymbol{H}}_j = \boldsymbol{H}_{\mathrm{w}}^{H}\boldsymbol{H}_{\mathrm{w}}$, and $\boldsymbol{A}_j = \boldsymbol{H}_{\mathrm{w}}\bar{\boldsymbol{F}}_{\mathrm{RF}}^{j}(\bar{\boldsymbol{F}}_{\mathrm{RF}}^{j})^{H}\boldsymbol{H}_{\mathrm{w}}^{H}$, where $\bar{\boldsymbol{F}}_{\mathrm{RF}}^{j}$ denotes a matrix obtained from $\boldsymbol{F}_{\mathrm{RF}}$ with its j-th column $\boldsymbol{f}_{\mathrm{RF}}^{(j)}$ removed.

Since all the elements in $\boldsymbol{F}_{\mathrm{RF}}$ other than $\boldsymbol{F}_{\mathrm{RF}}(i, j)$ are fixed, $\boldsymbol{A}_j$, $\zeta_{ij}^{\tilde{H}}$ and $\eta_{ij}^{\tilde{H}}$ seen in (20) are complex constants. Furthermore, under the modulus constraint of the analog precoder, i.e., $\boldsymbol{F}_{\mathrm{RF}}(i, j) = e^{-j\theta_{ij}}$, (20) can be re-stated as

$$g(\theta_{ij}) = \mathrm{Tr}(\boldsymbol{A}_j) + \zeta_{ij}^{\tilde{H}} + 2\mathrm{Re}\{\eta_{ij}^{\tilde{H}} e^{j\theta_{ij}}\}$$
$$= \mathrm{Tr}(\boldsymbol{A}_j) + \zeta_{ij}^{\tilde{H}} + \eta_{ij}^{\tilde{H}} e^{j\theta_{ij}} + (\eta_{ij}^{\tilde{H}})^{*} e^{-j\theta_{ij}} \quad (21)$$

Now the optimization is converted to an extreme-value problem, which can be readily solved. In detail, upon taking the derivative of $g(\theta_{ij})$ with respect to θ_{ij}, we obtain $\frac{\partial g(\theta_{ij})}{\partial \theta_{ij}} = j\eta_{ij}^{\tilde{H}} e^{j\theta_{ij}} - j(\eta_{ij}^{\tilde{H}})^{*} e^{-j\theta_{ij}} = 0$, which is equivalent to

$$\mathrm{Re}\{\eta_{ij}^{\tilde{H}}\}\sin(\theta_{ij}) + \mathrm{Im}\{\eta_{ij}^{\tilde{H}}\}\cos(\theta_{ij}) = 0 \quad (22)$$

Let us represent it in the form of

$$|\eta_{ij}^{\tilde{H}}|\sin(\theta_{ij} + \phi_{ij}) = 0 \quad (23)$$

where

$$\phi_{ij} = \begin{cases} \sin^{-1}\left(\dfrac{\mathrm{Im}\{\eta_{ij}^{\tilde{H}}\}}{|\eta_{ij}^{\tilde{H}}|}\right), & \text{if } \mathrm{Re}\{\eta_{ij}^{\tilde{H}}\} \geq 0, \\[3mm] \pi - \sin^{-1}\left(\dfrac{\mathrm{Im}\{\eta_{ij}^{\tilde{H}}\}}{|\eta_{ij}^{\tilde{H}}|}\right), & \text{if } \mathrm{Re}\{\eta_{ij}^{\tilde{H}}\} < 0 \end{cases} \quad (24)$$

Solving (24) under the constraint of $\theta_{ij} \in (0, 2\pi)$, we obtain

$$\theta_{ij}^{(1)} = -\phi_{ij},$$
$$\theta_{ij}^{(2)} = \pi - \phi_{ij}. \quad (25)$$

However, there is only one solution yielding a minimum value of $g(\theta_{ij})$, i.e., the optimum solution. Hence, the final solution to θ_{ij} is given by

$$\theta_{ij}^{(\mathrm{opt})} = \underset{\theta_{ij}^{(1)}, \theta_{ij}^{(2)}}{\arg\min}\left(g(\theta_{ij}^{(1)}), g(\theta_{ij}^{(2)})\right) \quad (26)$$

The above optimization process is repeated with respect to each of the elements in $\boldsymbol{F}_{\mathrm{RF}}$, and the elements of $\boldsymbol{F}_{\mathrm{RF}}$

are iteratively optimized until the cost function converges to a local minimum. Hence, before reaching the minimum, SI can be gradually suppressed with the increase of the number of iterations. A shortcoming of the CDC algorithm is that convergence is usually slow and dependent on the cost function of (18a), which in turn related to the SI channel and antenna configurations [27]. Nevertheless, once the condition of (18c) is satisfied, meaning that the SI reduction provided by beamforming is sufficient to make ADC work efficiently, more iterations for further SI reduction is no longer necessary. Hence, once the constraint of (18c) is met, the process of SI suppression can be terminated to save time. In Section V-A, we will demonstrate the convergence performance of the CDC algorithm.

In summary, the first design option is stated as Algorithm 1. For UL reception, when given $\boldsymbol{W}_{\mathrm{MMSE}}[\bar{m}]$, the hybrid combiner is obtained by the PGD algorithm. For SI suppression, after the initialization of $\boldsymbol{F}_{\mathrm{RF}}$, the analog precoder is iteratively updated to reduce the SI power based on the CDC algorithm, until the SIC meets the requirement. During every iteration, the digital precoder $\boldsymbol{F}_{\mathrm{BB}}[m]$ is derived based on ZF method and water-filling algorithm.

Algorithm 1 Precoding Optimization Aided SIC (Option 1)

Require: P_m, P_{DL}, $C_{\mathrm{SI}}^{\mathrm{Demand}}$
1: Compute $\boldsymbol{W}_{\mathrm{BB}}[\bar{m}]$ and $\boldsymbol{W}_{\mathrm{RF}}$ by the PGD method after obtaining $\boldsymbol{W}_{\mathrm{MMSE}}[\bar{m}]$ in (16).
2: Initialize $\boldsymbol{F}_{\mathrm{RF}}$.
3: **for** $1 \leq j \leq N_{\mathrm{RF}}$, **do**
4:     **for** $1 \leq i \leq N$, **do**
5:         Calculate $\eta_{ij}^{\tilde{H}}$ and $g(\theta_{ij})$ in (20) and (21), respectively;
6:         Derive $\theta_{ij}^{(1)}$ and $\theta_{ij}^{(2)}$ via minimizing $g(\theta_{ij})$;
7:         Find $\theta_{ij}^{(\mathrm{opt})} := \arg\min\left(g(\theta_{ij}^{(1)}), g(\theta_{ij}^{(2)})\right)$;
8:         $\boldsymbol{F}_{\mathrm{RF}}(i, j) = e^{-j\theta_{ij}^{(\mathrm{opt})}}$;
9:     **end for**
10: **end for**
11: **for** $1 \leq m \leq M$, **do**
12:     Derive $\boldsymbol{P}[m]$ based on the water-filling algorithm;
13:     Compute $\boldsymbol{F}_{\mathrm{BB}}^{\mathrm{ZF}}[m] = \boldsymbol{H}_{\mathrm{eq}}^{H}[m](\boldsymbol{H}_{\mathrm{eq}}[m]\boldsymbol{H}_{\mathrm{eq}}^{H}[m])^{-1}$ $\times\boldsymbol{P}^{\frac{1}{2}}[m]$, where $\boldsymbol{H}_{\mathrm{eq}}[m] = \boldsymbol{H}_{\mathrm{DL}}[m]\boldsymbol{F}_{\mathrm{RF}}$;
14: **end for**
15: Calculate the power of SI: $P_{\mathrm{SI}} = \sum_{m=1}^{M} \mathbb{E}\|\boldsymbol{y}_{\mathrm{SI}}[m]\|_2^2$.
16: **If** $\frac{P_{\mathrm{DL}}}{P_{\mathrm{SI}}} \geq 10^{\frac{C_{\mathrm{SI}}^{\mathrm{Demand}}}{10}}$, $\forall m$, store $\boldsymbol{F}_{\mathrm{RF}}$ and $\boldsymbol{F}_{\mathrm{BB}}^{\mathrm{ZF}}[m]$.
17: **Else**, go to Step 3.

B. COMBINING OPTIMIZATION AIDED SELF-INTERFERENCE CANCELLATION

In the context of the second design option, we assume that $\bar{N} > N$. In this scenario, the analog precoder $\boldsymbol{F}_{\mathrm{RF}}$ is derived via maximizing the DL spectral efficiency without considering the effect of the SI on the UL receiving. Instead,

SI suppression is only attempted by the design of $\boldsymbol{W}_{\text{RF}}$. Therefore, the design of the hybrid combiner in Option 2 is similar to the design of the hybrid precoder in Option 1, except that there is no power allocation in combiner's design. Furthermore, the analog and digital precoders in Option 2 can be designed by employing the PGD algorithm, when an overall precoder in the form of (19) is prepared.

It can be argued that the design in Option 2 has lower complexity than that in Option 1. The reason is that in Option 1, the digital precoder and analog precoder need to be iteratively updated, so that the SI on the UL receiving is gradually reduced to an allowed value. By contrast, in Option 2, once the hybrid DL precoder is obtained, the SI on UL receiver becomes stable. Hence, no iteration is required between the design of the digital combiner and that of the analog combiner. In other words, the analog combiner can be firstly designed to suppress SI to a sufficient level. Then, digital combiner can be derived for a fixed analog combiner. In summary, the design in Option 2 is stated as Algorithm 2.

Algorithm 2 Combining Optimization Aided SIC (Option 2)

Require: $P_m, P_{\text{DL}}, C_{\text{SI}}^{\text{Demand}}$
1: Derive full-digital precoder $\boldsymbol{F}^{\text{ZF}}[m]$ and divide it into $\boldsymbol{F}_{\text{RF}}$ and $\boldsymbol{F}_{\text{BB}}[m]$ based on PGD
2: Initialize $\boldsymbol{W}_{\text{RF}}$.
3: Design $\boldsymbol{W}_{\text{RF}}$ by following Step 3 to Step 10 in Algorithm 1.
4: Calculate the power of SI: $P_{\text{SI}} = \sum_{m=1}^{M} \mathbb{E} \left\| \boldsymbol{y}_{\text{SI}}[m] \right\|_2^2$.
5: **If** $\frac{P_{\text{DL}}}{P_{\text{SI}}} \geq 10^{\frac{C_{\text{SI}}^{\text{Demand}}}{10}}$, $\forall m$, store $\boldsymbol{W}_{\text{RF}}$;
6: **Else**, go to Step 3.
7: **for** $1 \leq m \leq \bar{M}$, **do**
8:    Compute $\boldsymbol{W}_{\text{BB}}[\bar{m}] = \left(\boldsymbol{H}_{\text{eq}}[\bar{m}] \boldsymbol{H}_{\text{eq}}^H[\bar{m}] + \sigma^2 \boldsymbol{I} \right)^{-1}$
   $\times \boldsymbol{H}_{\text{eq}}[\bar{m}]$, where $\boldsymbol{H}_{\text{eq}}[\bar{m}] = \boldsymbol{W}_{\text{RF}}^H \boldsymbol{H}_{\text{UL}}[\bar{m}]$;
9: **end for**

It is worth noting that following Options 1 and 2, there is a third option for the design, which optimizes $\boldsymbol{W}_{\text{RF}}$ and $\boldsymbol{F}_{\text{RF}}$ jointly. However, it can be shown that the SIC performance is mainly determined by the DL transmitter or UL receiver, depending on which of them has more antenna elements. As demonstrated in Section V, the side (either DL transmitter or UL receiver) with less antenna elements can hardly provide any gain for SIC. Owing to this, the third design option is not further considered in this paper.

IV. CHANNEL ESTIMATION IN MDD/MU-MIMO SYSTEMS

As argued in Section I of introduction, in MDD/MU-MIMO systems, the DL channels can be estimated based on the observations received from the UL channels by exploiting the reciprocity existing between the DL and UL sub-channels, which is generated by the frequency-domain correlated fading. In this section, we consider the CEst in MDD/MU-MIMO systems. We first consider the CEst

based on orthogonal transmission and focus on the design of frequency-domain pilot symbol (PS) vectors and the associated conditions. Then, the CEst in the scenario of non-orthogonal transmission is considered. Note that, below we only consider the CEst of communication channels. The SI channel can be estimated by the various approaches proposed in references, e.g., in [46]–[49].

By observing (2), (3) and (4), we can know that the CEst can be initialized with the UL training in frequency-domain. Using the frequency-domain training, the time-domain channel $\boldsymbol{g}_{n,d}$ can be estimated. Then, from $\boldsymbol{g}_{n,d}$ both the DL and UL channels of the subcarriers can be obtained with the aid of (3) and (4).

Let us assume that all MSs synchronously transmit their PSs. For CEst, we assume that each MS transmits PSs on all the UL subcarriers. The fading of channels is assumed to be slow enough for making use of the reciprocity for UL/DL processing. Then, consider that the PSs transmitted by the d-th MS are given by $\boldsymbol{x}_d = \left[x_d[1], \ldots, x_d[\bar{m}], \ldots, x_d[\bar{M}] \right]^T$, where d is either a UL MS or a DL MS. The received signal from the $\bar{m}$-th subcarrier by the n-th antenna (either the transmit or receive antenna at BS) can be expressed as

$$y_n[\bar{m}] = \sqrt{\rho_r} \sum_{d=1}^{D_{\text{sum}}} h_{n,d}[\bar{m}] x_d[\bar{m}] + z_n[\bar{m}],$$

$$\bar{m} = 1, \ldots, \bar{M} \quad (27)$$

where $z_n[\bar{m}] \sim \mathcal{CN}(0, \sigma^2)$ is the additive complex Gaussian noise, ρ_r represents the average transmit power per symbol per MS. Let $\boldsymbol{y}_n = \left[y_n[1], \ldots, y_n[\bar{M}] \right]^T$. Then, we can have an expression of

$$\boldsymbol{y}_n = \sqrt{\rho_r} \sum_{d=1}^{D_{\text{sum}}} \boldsymbol{X}_d \boldsymbol{h}_{n,d}^{\text{UL}} + \boldsymbol{z}_n$$

$$= \sqrt{\rho_r} \sum_{d=1}^{D_{\text{sum}}} \boldsymbol{X}_d \boldsymbol{\Phi}_{\text{UL}}^T \boldsymbol{F} \boldsymbol{\Psi} \boldsymbol{g}_{n,d} + \boldsymbol{z}_n \quad (28)$$

where $\boldsymbol{X}_d = \text{diag}\{\boldsymbol{x}_d\}$, $\boldsymbol{z}_n \sim \mathcal{CN}(\boldsymbol{0}, \sigma^2 \boldsymbol{I}_{\bar{M}})$, $\boldsymbol{h}_{n,d}^{\text{UL}}$ is given by (4), and with the aid of (2), i.e., $\boldsymbol{h}_{n,d}^{\text{UL}} = \boldsymbol{\Phi}_{\text{UL}}^T \boldsymbol{F} \boldsymbol{\Psi} \boldsymbol{g}_{n,d}$, $\boldsymbol{y}_n$ is directly expressed in terms of the TDCIR $\boldsymbol{g}_{n,d}$.

From (28), we can see that if the PSs can be designed to satisfy

$$\begin{cases} \left(\boldsymbol{X}_i \boldsymbol{\Phi}_{\text{UL}}^T \boldsymbol{F} \boldsymbol{\Psi} \right)^H \left(\boldsymbol{X}_i \boldsymbol{\Phi}_{\text{UL}}^T \boldsymbol{F} \boldsymbol{\Psi} \right) = \varrho \boldsymbol{I}_L, \\ \left(\boldsymbol{X}_i \boldsymbol{\Phi}_{\text{UL}}^T \boldsymbol{F} \boldsymbol{\Psi} \right)^H \left(\boldsymbol{X}_j \boldsymbol{\Phi}_{\text{UL}}^T \boldsymbol{F} \boldsymbol{\Psi} \right) = \boldsymbol{0}_L, \ \forall i \neq j \end{cases} \quad (29)$$

where ϱ is a constant, then the TDCIR $\boldsymbol{g}_{n,i}$ from MS i can be readily estimated by the LS method, given by

$$\hat{\boldsymbol{g}}_{n,i} = \frac{1}{\varrho \sqrt{\rho_r}} \left(\boldsymbol{X}_i \boldsymbol{\Phi}_{\text{UL}}^T \boldsymbol{F} \boldsymbol{\Psi} \right)^H \boldsymbol{y}_n \quad (30)$$

Furthermore, if MS i is a UL user and Antenna n is the receive antenna at BS, then BS uses (4) to obtain the frequency-domain channel gains for UL detection. By contrast, if MS i is a DL user and Antenna n is the

B. Li *et al.*: Self-Interference Cancellation and Channel Estimation in Multicarrier-Division Duplex Systems With Hybrid Beamforming

IEEE *Access*

transmit antenna of BS, then BS uses (3) to obtain the frequency-domain channel gains for DL precoding.

The set of PSs satisfying (30) are referred to as the orthogonality-achieving PSs. With the aid of the approach proposed in [50], it can be shown that if $\bar{M} \geq LD_{\text{sum}}$ and the $\bar{M}$ UL subcarriers are evenly distributed among the M_{sum} subcarriers, the set of PSs given by

$$\boldsymbol{x}_d = \left[1, e^{j2\pi \frac{(d-1)\xi}{\bar{M}}}, e^{j2\pi \frac{2(d-1)\xi}{\bar{M}}}, \cdots, e^{j2\pi \frac{(\bar{M}-1)(d-1)\xi}{\bar{M}}} \right]^T,$$
$$1 \leq d \leq D_{\text{sum}} \quad (31)$$

where $\xi = \left\lfloor \frac{\bar{M}}{D_{\text{sum}}} \right\rfloor$, are orthogonality-achieving PSs. Hence, we have the following Proposition.

Proposition 1: When $\xi = \left\lfloor \frac{\bar{M}}{D_{\text{sum}}} \right\rfloor \geq L$, and the $\bar{M}$ number of UL subcarriers are evenly distributed with a spacing of $l = M_{\text{sum}}/\bar{M}$, the D_{sum} PSs given in (31) make the matrices $\boldsymbol{P}[d] = \boldsymbol{X}_d \boldsymbol{\Phi}_{\text{UL}}^T \boldsymbol{F} \boldsymbol{\Psi}$ for $d = 1, \ldots, D_{\text{sum}}$ mutually orthogonal.

Proof: See Appendix. □

However, if the conditions stated in Proposition 1 are not satisfied, or more random PSs are used, orthogonality-achieving PSs may not be available. In this case, we can write (28) as

$$\boldsymbol{y}_n = \boldsymbol{Q}_i \boldsymbol{g}_{n,i} + \boldsymbol{T}_i + \boldsymbol{z}_n \quad (32)$$

where by definition, $\boldsymbol{Q}_i = \sqrt{\rho_r} \boldsymbol{X}_i \boldsymbol{\Phi}_{\text{UL}}^T \boldsymbol{F} \boldsymbol{\Psi}$, and $\boldsymbol{T}_i = \sqrt{\rho_r} \sum_{d=1, d \neq i}^{D_{\text{sum}}} \boldsymbol{X}_d \boldsymbol{\Phi}_{\text{UL}}^T \boldsymbol{F} \boldsymbol{\Psi} \boldsymbol{g}_{n,d}$ is the interference signal from other MSs. In order to suppress the interference from the other MSs, let us introduce the LMMSE estimator for CEst. Then, the estimate to $\boldsymbol{g}_{n,i}$ in (28) can be expressed as $\hat{\boldsymbol{g}}_{n,i} = \boldsymbol{A}_{n,i}^H \boldsymbol{y}_n$, where $\boldsymbol{A}_{n,i}$ achieving MMSE can be obtained from the minimization problem formulated as

$$\boldsymbol{A}_{n,i}^{\text{LMMSE}} = \arg \min_{\boldsymbol{A}} E \left[\left\| \boldsymbol{g}_{n,i} - \boldsymbol{A}^H \boldsymbol{y}_n \right\|^2 \right] \quad (33)$$

Assume that the TDCIRs from MSs are uncorrelated, i.e., $E[\boldsymbol{g}_{n,d} \boldsymbol{g}_{n,d'}^H] = \boldsymbol{0}, \forall d \neq d'$, which is usually satisfied as MSs are in general well separated in space. Then, the solution to (33) is

$$\boldsymbol{A}_{n,i}^{\text{LMMSE}} = \left(\frac{1}{L} \boldsymbol{Q}_i \boldsymbol{Q}_i^H + E[\boldsymbol{T}_i \boldsymbol{T}_i^H] + \sigma^2 \boldsymbol{I}_{\bar{M}} \right)^{-1} \left(\frac{1}{L} \boldsymbol{Q}_i \right) \quad (34)$$

where $E[\boldsymbol{T}_i \boldsymbol{T}_i^H] = \frac{\rho_r}{L} \sum_{d=1, d \neq i}^{D_{\text{sum}}} \boldsymbol{X}_d \boldsymbol{\Phi}_{\text{UL}}^T \boldsymbol{F} \boldsymbol{\Psi} \boldsymbol{\Psi}^H \boldsymbol{F}^H \boldsymbol{\Phi}_{\text{UL}}^* \boldsymbol{X}_d^H$. Correspondingly, the estimate $\hat{\boldsymbol{g}}_{n,i}$ is given by

$$\hat{\boldsymbol{g}}_{n,i} = \frac{1}{L} \boldsymbol{Q}_i^H \left(\frac{1}{L} \boldsymbol{Q}_i \boldsymbol{Q}_i^H + E[\boldsymbol{T}_i \boldsymbol{T}_i^H] + \sigma^2 \boldsymbol{I}_{\bar{M}} \right)^{-1} \boldsymbol{y}_n \quad (35)$$

It is well-known that LMMSE yields biased estimation. To attain an unbiased estimator, we can form the estimate as

$$\check{\boldsymbol{g}}_{n,i} = \left[\left(\boldsymbol{A}_{n,i}^{\text{LMMSE}} \right)^H \boldsymbol{Q}_i \right]^{-1} \hat{\boldsymbol{g}}_{n,i} \quad (36)$$

Again, after obtaining the estimation of $\check{\boldsymbol{g}}_{n,i}$, if MS i is a UL user and Antenna n is the UL receive antenna at BS,

BS uses (4) to obtain the frequency-domain channel for UL detection. By contrast, if MS i is a DL user and Antenna n is the DL transmit antenna at BS, BS uses (3) to obtain the frequency-domain channel for DL precoding.
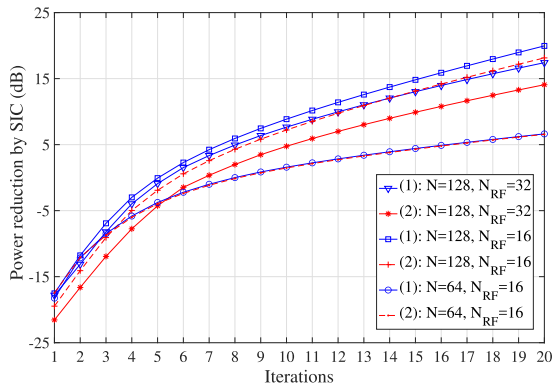
V. PERFORMANCE RESULTS

In this section, we first evaluate the SIC performance. Then, under the assumption of ideal CEst, the performance results for the MDD/MU-MIMO systems are depicted and discussed, when the precoder and combiner designed in Section III are employed. Then, the performance of the CEst method introduced in Section IV is investigated. Finally, we present the simulation results for the MDD/MU-MIMO systems when the LS and LMMSE CEsts are employed.

In our simulations, we assume the channel model as presented in Section II-A, and the ULA at BS with the half-wavelength spacing between two adjacent antenna elements. The distance r_{ij} between the i-th element of transmitter and the j-th element of receiver is set according to [21] and the default angle between the transmitter array and receiver array is $\varphi = 120°$. We further assume that the number of CIR taps for communications channel is $L = 4$. For the SI channel, we set $\kappa = 20$ dB as a default value.
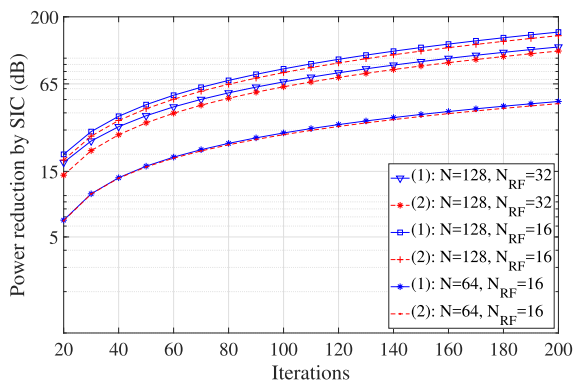
A. SELF-INTERFERENCE CANCELLATION

According to [51], we assume that the transmit power of BS and the signaling bandwidth are $P_{\text{DL}} = 30$ dBm and $B = 20$ MHz, respectively. The total transmit power is uniformly allocated to the DL subcarriers. We further assume the 12-bit ADCs used by the UL receiver at BS. Then, the maximum input power to the UL receiver and the demand of SIC can be found from (7) and (8), which are $s_{\text{max}} \approx -25$ dBm, $C_{\text{SI}}^{\text{Demand}} = 65$ dB, respectively. In other words, the system needs to achieve at least 65 dB of SI reduction, so that the UL receiver at BS can work efficiently.

In the first experiment, we demonstrate the SIC performance in the MDD/MU-MIMO systems with the transceivers designed under Option 1 of Section III. In this study, we assume that the number of antennas and RF chains at UL receiver are $\bar{N} = 32$ and $\bar{N}_{\text{RF}} = 8$, respectively. The other parameters are detailed under the caption of Fig. 2. In this figure, we compare the SIC performance of the proposed iterative coordinate descent algorithm, when the analog precoder is either randomly initialized or initialized via optimizing the DL sum-rate as in equation (19) in [40], which are referred to as the 'Random initial' and 'Optimized initial' analog precoders, respectively, in the figure. Note that the random initial analog precoder is obtained by firstly extracting the angle information from the null space matrix of $\boldsymbol{H}_{\text{SI}}$, i.e., from $\boldsymbol{V}_{(N-\text{rank}(\boldsymbol{H}_{\text{SI}})):\text{end}}$, and then, N_{RF} columns of $\boldsymbol{V}_{(N-\text{rank}(\boldsymbol{H}_{\text{SI}})):\text{end}}$ are randomly selected to construct F_{RF}. Note furthermore that the SIC behavior from the 1st to the 20th iterations are separately depicted in Fig. 2(a) to highlight the relatively sharp changes. As shown in Fig. 2, explicitly, the SI reduces with the increase of the number of iterations. Specifically, when BS employs $N = 128$ DL

IEEE *Access*

B. Li *et al.*: Self-Interference Cancellation and Channel Estimation in Multicarrier-Division Duplex Systems With Hybrid Beamforming
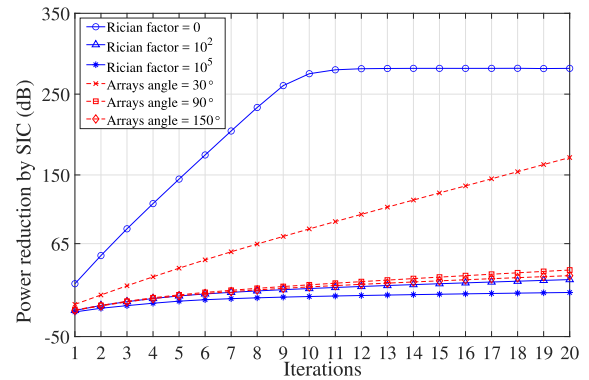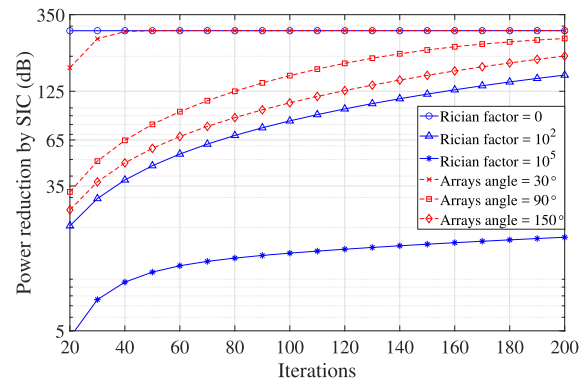

(a) Iterations: 1-20

(b) Iterations: 20-200

FIGURE 2. SI reduction versus number of iterations with P_{DL} = 30 dBm, B = 20 MHz, φ = 120°, κ = 20 dB. (1) Optimized initial analog precoder; (2) Random initial analog precoder.


(a) Iterations: 1-20

(b) Iterations: 20-200

FIGURE 3. SIC versus number of iterations performance with respect to different angles between the transmit and receive antenna arrays, as well as to different Rician factors of SI channel, when assuming P_{DL} = 30 dBm, B = 20 MHz, N = 128, $\bar{N}$ = 32, N_{RF} = 16 and $\bar{N}_{RF}$ = 8.

transmit antennas and N_{RF} = 16 DL RF chains, 65 dB of SIC reduction can be achieved after 80 iterations, when either the random initial or optimized initial analog precoder is employed. The performance achieved by the random initial analog precoder and optimized initial analog precoder is very similar. Fig. 2 illustrates that employing more DL transmit antennas allows more SI reduction for a given number of iterations. For N_{RF} = 16 and when the number of DL transmit antennas is decreased from 128 to 64, the SI reduction capability is reduced from about 65 dB to about 25 dB after 80 iterations. Furthermore, Fig. 2 shows that when the number of RF chains is reduced from 32 to 16 while keeping the number of DL transmit antennas fixed, more than 2.5 dB of SI reduction can be obtained. Note that, the above observations can be similarly obtained from the systems operated under Option 2, when the above-stated DL transmit antennas is changed to the UL receive antennas.

The second experiment considers the effect of the Rician factor κ and the arrays angle φ on the performance of SIC. Again, we assume that the system is operated under Option 1 with the parameters as shown in the caption of Fig. 3, where the range from the 1st to the 20th iterations are separately depicted in Fig. 3(a) for highlighting the behavior. It can be observed that the Rician factor and arrays angle

yield big impacts on the SIC performance. Specifically in terms of the Rician factor, it can be seen that when the LOS component becomes more dominant, the proposed SIC method becomes less efficient. However, we should note that while the beamforming methods work inefficiently with the LOS component, other easy-implementing approaches, such as, of adding blockage between transmitter and receiver [6], [52]–[55], may be employed to significantly mitigate the LoS SI. In terms of the angle between the transmit and receive antenna arrays, Fig. 3 shows that the narrower angel is set, the more SI can be reduced. This is because when the angle is narrower, the SI power imposed by the SI signal of a given transmit array element on all the receiver array elements is nearly same, which is beneficial to SIC by using beamforming technique. By contrast, if the angle between transmit/receive arrays is wide, the distances from a given transmit array element to all the receive antenna array elements can be very different. Hence, the SI power from a given transmit array element to the receive array elements is very different. Consequently, it is difficult for the beamformer to simultaneously suppress them efficiently.

Additionally, from Figs. 2 and 3 we can be implied that the SI reducing rate and the SIC potential provided by the

B. Li et al.: Self-Interference Cancellation and Channel Estimation in Multicarrier-Division Duplex Systems With Hybrid Beamforming

IEEE Access

proposed CDC algorithm are dependent on the antenna configuration and SI channel's characteristics. For instance, if the SI channel only has NLOS components, the CDC algorithm makes the SI approach a fixed value after about 10 iterations, yielding a SI reduction of about 300 dB, which is much larger than C_{SI}^{Demand} of required. As shown in Figs. 2 and 3, in some cases, the SI reducing rate is relatively small, but the CDC algorithm can still allow to achieve the required SIC. For example, when the Rician factor is 100, the algorithm is able to provide about 65 dB SI reduction after about 80 iterations. In some other cases, such as, when the Rician factor is 10^5, the SI reducing rate is very small and the SIC requirement of (18b) is hard to meet, even after many iterations. However, it is worth noting that in this case, the LoS propagation is dominant and the SI can be efficiently suppressed by the other approaches of, such as, using blockage. In summary, from the results of Figs. 2 and 3 we can know that to attain a good performance of SI reduction, we can increase the number of antennas at the side implementing SIC and/or reduce the angle between TX/RX antenna arrays.
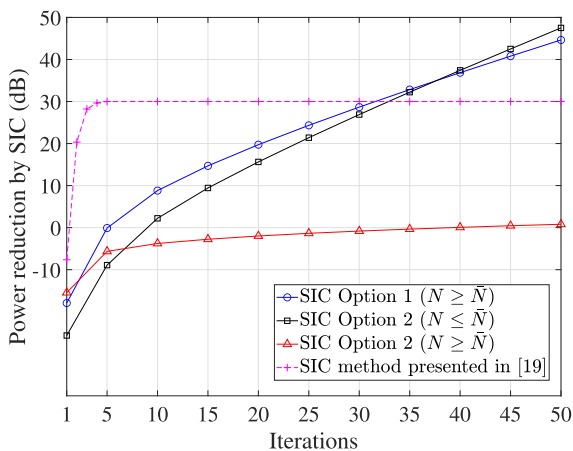
FIGURE 4. SIC performance comparison of the proposed methods with Option 1 and Option 2 and the method presented in [23], when $P_{DL} = 30$ dBm, $B = 20$ MHz, $\varphi = 120°$, and $\kappa = 20$ dB.

Finally, we compare the SIC performance of the MDD/MU-MIMO systems with the transceivers designed by Option 1 and Option 2, respectively, in Fig. 4. The beamforming based SIC algorithm presented in [23] is shown as the benchmark. In this study, we set the parameters to $N = 128$, $\bar{N} = 32$, $N_{RF} = 16$ and $\bar{N}_{RF} = 8$ for Option 1, for Option 2 in the case of $N \geq \bar{N}$ and also for the algorithm presented in [23]. For the Option 2 in the case of $N < \bar{N}$, we set $N = 32, \bar{N} = 128, N_{RF} = 8$, and $\bar{N}_{RF} = 16$. From Fig. 4 we observe that Option 1 and Option 2 are equally efficient for SI mitigation, when the same number of antennas used for SI suppression is assumed. Moreover, as shown in Fig. 4, in the case of $N \geq \bar{N}$, if Option 2 is employed to mitigate SI, i.e., SI is suppressed by receive antenna array, the SIC gain is very limited. Therefore, when given the deployment of $N \geq \bar{N}$ or $N \leq \bar{N}$, there is not much meaning to implement the joint transmit/receive

beamforming for SI mitigation. This is because in contrast to using either transmit beamforming in the case of $N \geq \bar{N}$ or receive beamforming under $N \leq \bar{N}$, the SIC gain provided by the joint transmit/receive beamforming is marginal, while the increase of implementation complexity is significant. Additionally, when comparing the SIC Option 1 with Fig. 2(b) in the case of (1): $N = 128$, $N_{RF} = 16$, both cases use the same parameters, we can see that the proposed algorithm is capable of providing 65 dB of required SI reduction after 80 iterations. By contrast, although the SIC algorithm presented in [23] can provide 30 dB SI reduction after 5 iterations, it however gets saturated at this value and is unable to achieve the required SI reduction in analog-domain, no matter how many iterations of the algorithm are executed.

TABLE 2. Comparison between the proposed and competing beamforming aided SIC method.

Method	Constraint	Complexity	SIC Capability
Option 1	$N \geq \bar{N}$	$\mathcal{O}(\bar{N}^3 + N\bar{N}\bar{N}_{RF})$	high
Option 2	$N \leq \bar{N}$	$\mathcal{O}(N\bar{N}\bar{N}_{RF})$	high
Option 2	$N \geq \bar{N}$	$\mathcal{O}(N\bar{N}\bar{N}_{RF})$	low
[23]	$N \geq \bar{N}$	$\mathcal{O}(\bar{N}^3 + NN_{RF}^2)$	medium

In Table 2, we summarize the comparison between the proposed SIC methods and the method presented in [23] in terms of their complexity and SIC capability. The complexity shown in Table 2 includes both the complexity for SI reduction and that for digital precoder/combiner, when the number of antenna elements and that of RF chains at transmitter or receiver are given. First, regarding to the SIC performance, as we stated in Section III-B, both Option 1 and Option 2 ($N \leq \bar{N}$) have the highest SIC capability. However, as the SIC is independent of the design of precoder, Option 2 ($N \leq \bar{N}$) demands lower computational complexity than Option 1. As shown in Table 2, Option 2 ($N \geq \bar{N}$) also has low computational complexity, but it is unable to provide sufficient SI suppression due to the constraint on antenna arrays, as shown in Fig 4. As for the method presented in [23], it can provide upto 30 dB SI reduction after about 5 iterations, but no further SI reduction is available, no matter how many iterations are executed. Hence, when taking into account the SIC capability and the required complexity, as shown in Table 2, Option 2 with $N \leq \bar{N}$ constitutes the most desirable SIC method.
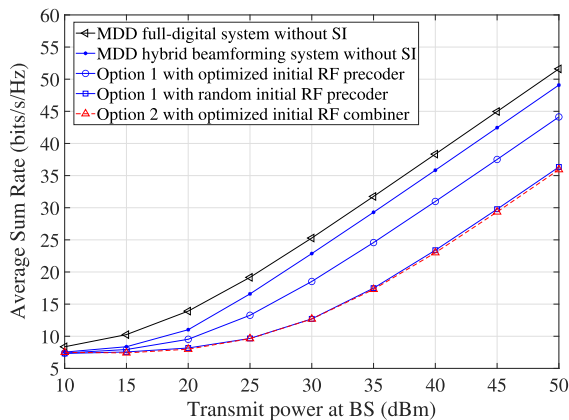
B. PERFORMANCE OF HYBRID MDD/MU-MIMO SYSTEMS WITH SI CANCELLATION

We now demonstrate the achievable performance of the hybrid MDD/MU-MIMO systems with SI Cancellation. For this purpose, we consider a MDD/MU-MIMO system, where BS employs $N = 128$ transmit antennas and $N_{RF} = 16$ DL RF chains to support $D = 6$ DL MSs, as well as $\bar{N} = 32$ receive antennas and $\bar{N}_{RF} = 8$ UL RF chains to serve $\bar{D} = 4$ UL MSs. Unless explicitly noted, the transmit power of BS and MS is set to $P_{DL} = 30$ dBm and $P_{MS} = 20$ dBm, respectively [51], [56]. Furthermore, at BS, the transmit power is

evenly assigned to the M DL subcarriers, while the transmit power of a DL subcarrier is assigned to the D number of DL MSs based on the water-filling principle. The total bandwidth is assumed to be 20 MHz and the number of DL and UL subcarriers are $M = 64$ and $\bar{M} = 32$, respectively. The MSs are assumed to be uniformly distributed within a circular area of radius $R = 60$ m. Furthermore, the pathloss for a MS with distance d from BS is modeled as $P_L(\text{dB}) = 72 + 29.2 \log_{10}(d)$. Additionally, the power spectral density of noise is -173 dBm/Hz. In the following figures, the average sum rate denotes the total rate of a system, including both DL and UL, which is formulated as

$$R_{\text{MDD}} = \frac{1}{M_{\text{sum}}} \left(\sum_{m=1}^{M} \sum_{d=1}^{D} R_d[m] + \sum_{\bar{m}=1}^{\bar{M}} \sum_{\bar{d}=1}^{\bar{D}} R_{\bar{d}}[\bar{m}] \right) \quad (37)$$

Note that the comprehensive comparison of MDD with TDD/IBFD in mmWave environment can be found in [12]. More general comparison of MDD with FDD/TDD can be found in [11]. Readers interested in the more details about the comparison are referred to these references.

FIGURE 5. Average sum-rate of the MDD/MU-MIMO systems with different beamforming/initialization schemes, when $N = 128$, $N_{\text{RF}} = 16$, $\bar{N} = 32$, $\bar{N}_{\text{RF}} = 8$, $M = 64$, $\bar{M} = 32$, $D = 6$, $\bar{D} = 4$ and $L = 4$.

Fig. 5 demonstrates the sum-rate performance of the MDD/MU-MIMO systems with various beamforming schemes. In this study, the transmit power at BS varies from 10 dBm to 50 dBm, while the transmit power of individual MSs is 20 dBm. From the results of Fig. 5, we observe that the ideal full-digital MDD/MU-MIMO system without SI provides the upper-bound performance. Note that, here 'without SI' means that the required SIC can be achieved by the easy-implementing SIC approach. However, when hybrid beamforming assisted SIC is considered, as Fig. 5 shows, using different initial analog precoders under Option 1 yield a big impact on the achievable sum-rate. The optimized initial analog precoder achieves much higher sum-rate than the random initial analog precoder. By contrast, when operated under Option 2, the optimized initial analog combiner can only achieve the similar performance of the Option 1 with random initial analog precoder. The reason behind is that in

this study, we assumed $\bar{N} \ll N$, and in this case, as argued in Section III, the performance of SIC should be dominated by the transmitter-based SIC, i.e., Option 1 design.
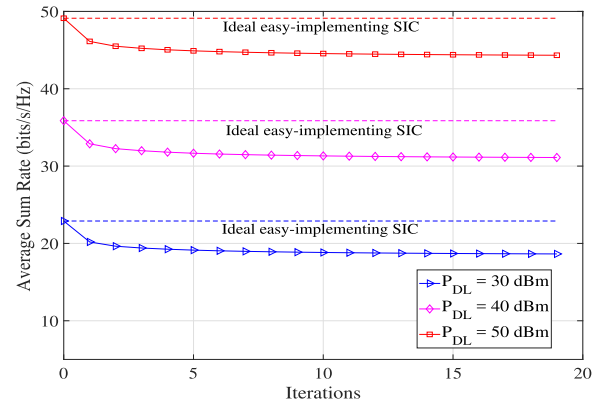
FIGURE 6. Average sum-rate versus the number of iterations of the analog precoder operated during the SIC process, when $N = 128$, $N_{\text{RF}} = 16$, $\bar{N} = 32$, $\bar{N}_{\text{RF}} = 8$, $M = 64$, $\bar{M} = 32$, $D = 6$, $\bar{D} = 4$ and $L = 4$.

Fig. 6 shows the impact of the number of iterations used by the analog precoder during SIC on the average sum-rate achieved. The SIC is achieved by the analog precoder operated under Option 1, and the parameters are detailed with the figure. For this figure, we assume that the remaining SI not suppressed by the analog precoder is ideally suppressed by the other easy-implementing approach. Therefore, as shown in Fig. 6, the highest sum-rate is observed before the analog precoder starts operating. When the analog precoder is operated with more iterations, the achieved sum-rate reduces, as the result that more degrees-of-freedom provided by transmit antennas are used for SIC. However, the achievable sum-rate becomes steady after only about 3 or 4 iterations, yielding the sum-rate cost for SIC. By contrast, as shown in Fig. 2, the amount of SI compressed monotonically increases with the increase of the number of iterations.
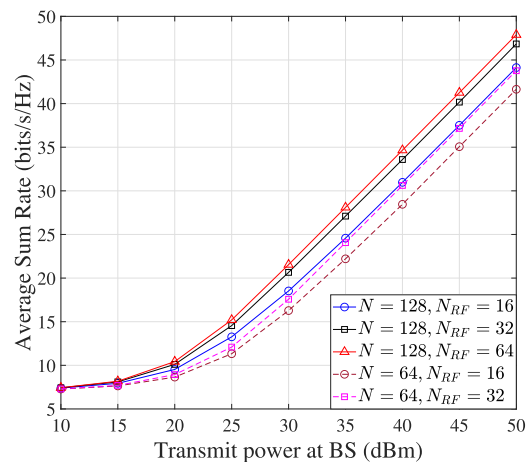
FIGURE 7. Average sum-rate versus BS's transmit power for the MDD/MU-MIMO systems employing different numbers of DL transmit antennas and RF chains.

The impact of the number of DL transmit antennas N and the number of DL RF chains N_{RF} on the sum-rate performance of MDD/MU-MIMO systems is shown in Fig. 7, when

B. Li et al.: Self-Interference Cancellation and Channel Estimation in Multicarrier-Division Duplex Systems With Hybrid Beamforming

IEEE *Access*

assuming that SI is suppressed using the Option 1 method. Explicitly, for a given number of DL transmit antennas, the achievable sum-rate increases, as the number of RF chains increases, which is at the cost of the increase of implementation complexity. By contrast, when N_{RF} is fixed, the sum-rate increases, as N increases, owing to the improved SI capability.
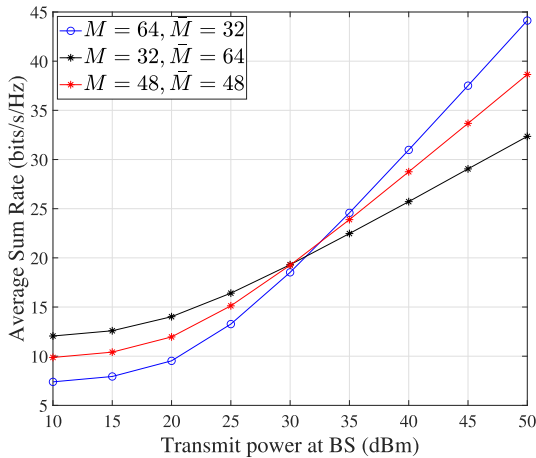

FIGURE 8. Average sum-rate versus BS's transmit power for the MDD/MU-MIMO systems employing different numbers of DL/UL subcarriers.

Fig. 8 depicts the effect of the numbers of DL/UL subcarriers, i.e., M and $\bar{M}$, on the sum-rate performance of MDD/MU-MIMO systems, when the total number of subcarriers is set to $M + \bar{M} = 128$, and the other parameters are set as default values. As each UL MS has fixed transmit power, while the total BS transmit power is shared by all DL MSs, the total throughput of MDD/MU-MIMO system is dominated by the UL, when the transmit power of BS is relatively low. In this case, when the UL employs more subcarriers, the total throughput of MDD/MU-MIMO system is higher. By contrast, when BS's transmit power is sufficiently high, the system's throughput will become DL dominant. Correspondingly, employing more DL subcarriers provides higher throughput by the MDD/MU-MIMO system.

By contrast, in Fig. 9, we investigate the effect of the numbers of DL/UL MSs, i.e., D and $\bar{D}$, on the sum-rate performance of MDD/MU-MIMO systems, while the other parameters are set to default values. As seen in Fig. 9, first, supporting more DL or/and UL MSs in general improves the total throughput of MDD/MU-MIMO systems. Second, when D is fixed, the total throughput of MDD/MU-MIMO systems increases, as the value of $\bar{D}$ increases. Finally, in the case that $\bar{D}$ is fixed, we observe that the total throughput achieved by $D = 12$ is slightly lower than that obtained by $D = 6$, when BS's transmit power is relatively low. However, when BS's transmit power is relatively high, the observation reverses, i.e., the total throughput achieved by $D = 12$ is higher than that obtained by $D = 6$. The reason behind this observation is that when at relatively low transmit power, the systems' total throughput is nominated by the UL MSs.
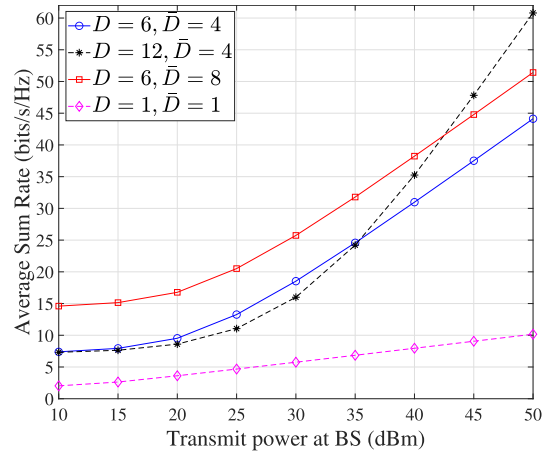

FIGURE 9. Average sum-rate versus BS's transmit power for the MDD/MU-MIMO systems employing different numbers of DL/UL users.

By contrast, at relatively high transmit power, the systems' total throughput is nominated by the DL MSs, owing to the contribution from the joint power-allocation among the DL MSs.
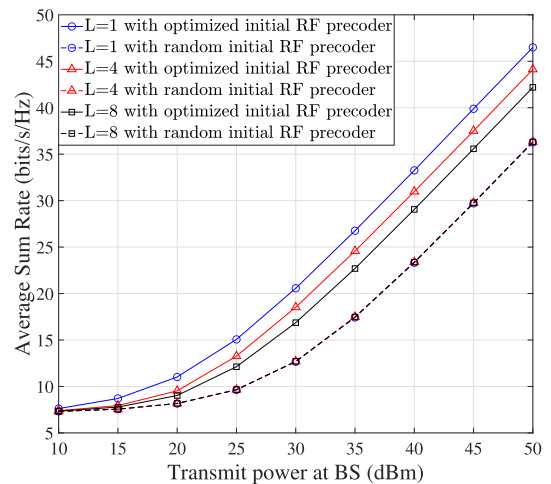

FIGURE 10. Average sum-rate performance of MDD/MU-MIMO systems experiencing the frequency-selective fading channels with different taps.

Fig. 10 shows the effect of the severity of frequency-selective fading channel on the achievable sum-rate performance of MDD/MU-MIMO systems, where increasing L means the channel becomes more frequency-selective. As shown in Fig. 10, when the optimized initial analog precoder is employed, the achieved sum-rate reduces with the increase of L. This is because when L increases, the fading experienced by different subcarriers becomes more random, making the optimized initial analog precoder appear more like the random initial analog precoder. By contrast, when the random initial analog precoder is employed, the achieved sum-rate is very similar, regardless of the values of L. Hence, while the random initial analog precoder usually achieves

lower sum-rate than the optimized initial analog precoder, it is more robust to the time-varying of channels.
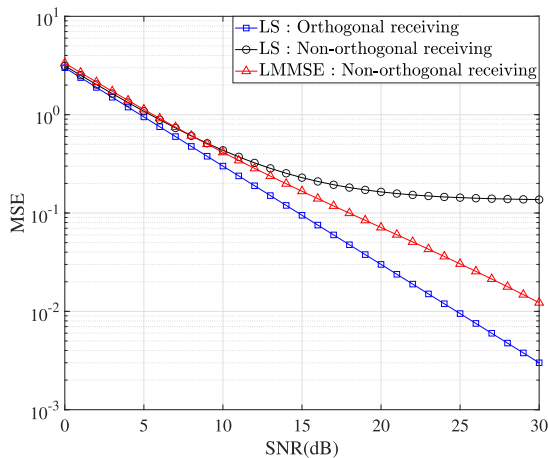
FIGURE 11. Mean-square error (MSE) performance of channel estimation in MDD/MU-MIMO systems, when $N = 128$, $\bar{N} = 32$, $M = 128$, $\bar{M} = 64$ and $L = 4$, and for LS $D = 6$ and $\bar{D} = 4$, while for LMMSE $D = 12$ and $\bar{D} = 6$.

C. CHANNEL ESTIMATION

In order to investigate the performance of CEst, we consider a MDD/MU-MIMO system where a BS employs a 128×32 antenna array, and the number of DL and UL subcarriers are $M = 128$ and $\bar{M} = 64$, respectively. Specifically in Fig. 11, we compare the MSE performance of CEst in three cases. In the first case, the LS CEst with orthogonality-achieving PSs, i.e., with the settings satisfying Proposition 1 is considered. In the second case, we also assume the LS CEst but with the UL subcarriers randomly selected. Therefore, the orthogonality-achieving PSs cannot be guaranteed. Finally, in the case of LMMSE CEst, the UL subcarriers are also randomly distributed. From Fig. 11 we observe that the LS CEst with orthogonality-achieving PSs achieves better MSE performance than the other two CEsts, while the LS CEst with randomly selected UL subcarriers achieves the worst MSE performance. Furthermore, the LS CEst with random UL subcarriers experiences the interference, which is unable to be suppressed by the method, hence yielding MSE floor. By contrast, the LMMSE CEst is capable of efficiently suppressing the interference and removing the MSE floor. We should note that, although the LS CEst with orthogonality-achieving PSs outperforms the LMMSE CEst in terms of MSE performance, it has the disadvantages of, such as, low number of orthogonality-achieving PSs due to the constraint of Proposition 1.

Finally, in Fig. 12 we compare the achievable sum-rate of MDD/MU-MIMO systems, when the channel knowledge is obtained by the LS CEst with orthogonality-achieving PSs or the LMMSE CEst with random UL subcarriers. Furthermore, the case of ideal CEst is included as a benchmark. Explicitly, both CEst schemes work efficiently over the SNR range considered. The sum-rate gap between that achieved by assuming ideal channel knowledge and that achieved by practical CEst is marginal. When comparing the LS and
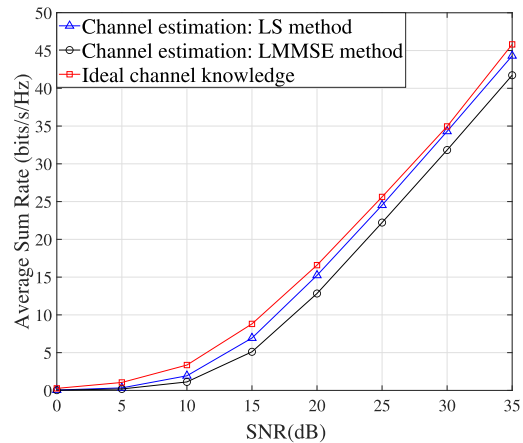
FIGURE 12. Average sum-rate versus SNR performance of MDD/MU-MIMO systems with channel knowledge provided by different methods. Parameters: $M = 128$, $\bar{M} = 64$, $L = 4$, $D = 8$ and $\bar{D} = 4$.

LMMSE methods, we find that the LS CEst allows to transmit an extra of 2.5 bits/s/Hz beyond the sum-rate achieved by the LMMSE CEst. However, we should remember the LS CEst with orthogonality-achieving PSs is limited by Proposition 1.

VI. CONCLUSION

In this paper, we have investigated the adaptive SIC methods based on the hybrid beamforming design of both transmitter and receiver as well as the CEst in MDD/MU-MIMO systems. We have first highlighted the design of the hybrid transmitter precoder for DL transmission and the hybrid receiver combiner for UL signal detection, both of which can simultaneously suppress SI to a desired level. Our studies show that SI can be dynamically mitigated by employing either the analog transmitter precoding or the analog receiver combining. Furthermore, it is shown that SIC should be implemented at BS transmitter or at BS receiver depending on which of them has more antenna elements. Then, the CEst in MDD/MU-MIMO systems has been designed by exploiting the reciprocality existing between UL/DL channels resulted from the correlated fading of subcarriers. Our studies reveal that first, when the number of MSs is relatively small and the PSs are evenly arranged across the subcarriers, the design of orthogonality-achieving PSs is available. In this case, a LS CEst achieves optimum performance. However, when randomly distributed PSs have to be used due to, such as, a big number of MSs, the performance of LS CEst degrades significantly. Instead, a LMMSE CEst is near-optimum, and is capable of significantly improving the performance over the LS CEst. Finally, the performance of the MDD/MU-MIMO systems with our proposed hybrid beamforming SIC method has been investigated, when CSI is provided by our proposed CEst, showing that the achievable performance can be close to that with ideal CSI.

MDD provides an opportunity for UL/DL channels to jointly share the frequency-domain resources. Our future work will consider the hybrid transceiver design in conjunction with joint UL/DL resource allocation in MDD/MU-MIMO systems.

B. Li *et al.*: Self-Interference Cancellation and Channel Estimation in Multicarrier-Division Duplex Systems With Hybrid Beamforming

IEEE*Access*

APPENDIX
(PROOF OF PROPOSITION 1)

Given that $\xi = \left\lfloor \frac{\bar{M}}{D_{\text{sum}}} \right\rfloor \geq L$, and the UL subcarriers are uniformly distributed with spacing of $l = M_{\text{sum}}/\bar{M}$ number of subcarriers between two adjacent UL subcarriers, we need to prove that

$$\boldsymbol{P}[m]^H \boldsymbol{P}[n] = \begin{cases} \boldsymbol{0}_L, & \text{if } m \neq n \\ \varrho \boldsymbol{I}_L, & \text{if } m = n \end{cases} \tag{38}$$

where $\boldsymbol{0}_L$ is a $(L \times L)$ all-zero matrix, and $\varrho = \bar{M}/M_{\text{sum}}$ is constant.

Since the UL subcarriers are uniformly-spaced with a spacing of l number of subcarriers between two adjacent UL subcarriers, it can be shown that the matrix $\boldsymbol{\Phi}_{\text{UL}}^T \boldsymbol{F} \boldsymbol{\Psi}$ is given by

$$\boldsymbol{G}_{\text{UL}} = \boldsymbol{\Phi}_{\text{UL}}^T \boldsymbol{F} \boldsymbol{\Psi}$$

$$= \frac{1}{M_{\text{sum}}} \begin{bmatrix} 1 & e^{-j2\pi \frac{(\bar{m}_1 - 1)}{M_{\text{sum}}}} & \cdots & e^{-j2\pi \frac{(\bar{m}_1 - 1)(L-1)}{M_{\text{sum}}}} \\ 1 & e^{-j2\pi \frac{(\bar{m}_2 - 1)}{M_{\text{sum}}}} & \cdots & e^{-j2\pi \frac{(\bar{m}_2 - 1)(L-1)}{M_{\text{sum}}}} \\ \vdots & \vdots & \cdots & \vdots \\ 1 & e^{-j2\pi \frac{(\bar{m}_{\bar{M}} - 1)}{M_{\text{sum}}}} & \cdots & e^{-j2\pi \frac{(\bar{m}_{\bar{M}} - 1)(L-1)}{M_{\text{sum}}}} \end{bmatrix}_{\bar{M} \times L} \tag{39}$$

where $\bar{m}_1, \bar{m}_2, \cdots, \bar{m}_{\bar{M}}$ are the indices of UL subcarriers. Note that, to obtain (39), the relationships of $\bar{m}_2 - \bar{m}_1 = \ldots = \bar{m}_{\bar{M}} - \bar{m}_{\bar{M}-1} = l$ are used. Let

$$\tilde{\boldsymbol{P}} = \boldsymbol{P}[m]^H \boldsymbol{P}[n] = (\boldsymbol{X}_m \boldsymbol{G}_{\text{UL}})^H (\boldsymbol{X}_n \boldsymbol{G}_{\text{UL}}),$$
$$1 \leq m, \ n \leq D_{\text{sum}} \tag{40}$$

Then, upon applying (31) and with the aid of (39), we can show that the (u, v)-th element of $\tilde{\boldsymbol{P}}$ is

$$\tilde{\boldsymbol{P}}(u, v) = \frac{1}{M_{\text{sum}}} \sum_{t=1}^{\bar{M}} (\boldsymbol{X}_m[t, t])^* (\boldsymbol{X}_n[t, t]) e^{\frac{j2\pi(\bar{m}_t - 1)(u-v)}{M_{\text{sum}}}}$$

$$= \frac{1}{M_{\text{sum}}} \sum_{t=1}^{\bar{M}} e^{\frac{j2\pi(t-1)(n-m)\xi}{\bar{M}}} e^{\frac{j2\pi(\bar{m}_t - 1)(u-v)}{M_{\text{sum}}}}$$

$$\overset{(a)}{=} \frac{1}{M_{\text{sum}}} \sum_{t=1}^{\bar{M}} e^{\frac{j2\pi(t-1)(n-m)\xi}{\bar{M}}} e^{\frac{j2\pi(t-1)(u-v)}{\bar{M}}}$$

$$= \frac{1}{M_{\text{sum}}} \sum_{t=1}^{\bar{M}} e^{\frac{j2\pi(t-1)[(n-m)\xi + u - v]}{\bar{M}}}$$

$$= \frac{\bar{M}}{M_{\text{sum}}} \delta[\Delta_{uv} - (m-n)\xi] \tag{41}$$

where $\Delta_{uv} = u - v$. In (41), and Equation (a) is because of $l = M_{\text{sum}}/\bar{M}$.

Explicitly, $\tilde{\boldsymbol{P}}(u, v) = \bar{M}/M_{\text{sum}}$ provided that $\Delta_{uv} - (m-n)\xi = 0$. Hence, when $m = n$, we have $\tilde{\boldsymbol{P}}(u, u) = \bar{M}/M_{\text{sum}}$ and $\tilde{\boldsymbol{P}}(u, v) = 0$ for all $u \neq v$. Therefore, $\boldsymbol{P}[m]^H \boldsymbol{P}[m] = \varrho \boldsymbol{I}_L$ with $\varrho = \bar{M}/M_{\text{sum}}$.

By contrast, in the case of $m \neq n$, since $\tilde{\boldsymbol{P}}$ is a $(L \times L)$ matrix, we have $-(L-1) \leq \Delta_{uv} \leq L-1$. Hence, $\Delta_{uv} - (m-n)\xi \neq 0$, provided that $\xi \geq L$. Therefore, we have $\boldsymbol{P}[m]^H \boldsymbol{P}[n] = \boldsymbol{0}_L$ for all $m \neq n$, provided that $\xi \geq L$.

In summary, when given $\xi \geq L$ and that the UL subcarriers are uniformly arranged with a constant spacing of l between two adjacent UL subcarriers, the set of PSs given by (31) satisfy (38), i.e., they are the orthogonality-achieving PSs.

REFERENCES

[1] J. G. Andrews, S. Buzzi, W. Choi, S. V. Hanly, A. Lozano, A. C. K. Soong, and J. C. Zhang, "What will 5G be?" *IEEE J. Sel. Areas Commun.*, vol. 32, no. 6, pp. 1065–1082, Jun. 2014.

[2] V. W. Wong, *Key Technologies for 5G Wireless Systems*. Cambridge, U.K.: Cambridge Univ. Press, 2017.

[3] J. Flordelis, F. Rusek, F. Tufvesson, E. G. Larsson, and O. Edfors, "Massive MIMO performance—TDD versus FDD: What do measurements say?" *IEEE Trans. Wireless Commun.*, vol. 17, no. 4, pp. 2247–2261, Apr. 2018.

[4] D. Kim, H. Lee, and D. Hong, "A survey of in-band full-duplex transmission: From the perspective of PHY and MAC layers," *IEEE Commun. Surveys Tuts.*, vol. 17, no. 4, pp. 2017–2046, 4th Quart., 2015.

[5] A. Sabharwal, P. Schniter, D. Guo, D. W. Bliss, S. Rangarajan, and R. Wichman, "In-band full-duplex wireless: Challenges and opportunities," *IEEE J. Sel. Areas Commun.*, vol. 32, no. 9, pp. 1637–1652, Sep. 2014.

[6] K. E. Kolodziej, B. T. Perry, and J. S. Herd, "In-band full-duplex technology: Techniques and systems survey," *IEEE Trans. Microw. Theory Techn.*, vol. 67, no. 7, pp. 3025–3041, Jul. 2019.

[7] M. Duarte and A. Sabharwal, "Full-duplex wireless communications using off-the-shelf radios: Feasibility and first results," in *Proc. Conf. Rec. 44th Asilomar Conf. Signals, Syst. Comput.*, Nov. 2010, pp. 1558–1562.

[8] B. Debaillie, D.-J. van den Broek, C. Lavin, B. van Liempd, B. Nauta, E. A. M. Klumperink, C. Palacios, J. Craninckx, and A. Parssinen, "Analog/RF solutions enabling compact full-duplex radios," *IEEE J. Sel. Areas Commun.*, vol. 32, no. 9, pp. 1662–1673, Sep. 2014.

[9] N. M. Gowda and A. Sabharwal, "JointNull: Combining partial analog cancellation with transmit beamforming for large-antenna full-duplex wireless systems," *IEEE Trans. Wireless Commun.*, vol. 17, no. 3, pp. 2094–2108, Mar. 2018.

[10] L.-L. Yang, *Multicarrier Communications*. Hoboken, NJ, USA: Wiley, 2009.

[11] L.-L. Yang, "Multicarrier-division duplexing (MDD): A duplexing scheme whose time has come," *IEEE COMSOC MMTC E-Lett.*, vol. 10, pp. 35–38, Jan. 2015.

[12] R. Rajashekar, C. Xu, N. Ishikawa, L.-L. Yang, and L. Hanzo, "Multicarrier division duplex aided millimeter wave communications," *IEEE Access*, vol. 7, pp. 100719–100732, 2019.

[13] K. T. Truong and R. W. Heath, Jr., "Effects of channel aging in massive MIMO systems," *J. Commun. Netw.*, vol. 15, no. 4, pp. 338–351, Aug. 2013.

[14] T. Riihonen, A. Balakrishnan, K. Haneda, S. Wyne, S. Werner, and R. Wichman, "Optimal eigenbeamforming for suppressing self-interference in full-duplex MIMO relays," in *Proc. 45th Annu. Conf. Inf. Sci. Syst.*, Mar. 2011, pp. 1–6.

[15] I. Atzeni and M. Kountouris, "Full-duplex MIMO small-cell networks with interference cancellation," *IEEE Trans. Wireless Commun.*, vol. 16, no. 12, pp. 8362–8376, Dec. 2017.

[16] T. Riihonen, S. Werner, and R. Wichman, "Mitigation of loopback self-interference in full-duplex MIMO relays," *IEEE Trans. Signal Process.*, vol. 59, no. 12, pp. 5983–5993, Dec. 2011.

[17] Y. Hua, P. Liang, Y. Ma, A. C. Cirik, and Q. Gao, "A method for broadband full-duplex MIMO radio," *IEEE Signal Process. Lett.*, vol. 19, no. 12, pp. 793–796, Dec. 2012.

[18] P. Lioliou, M. Viberg, M. Coldrey, and F. Athley, "Self-interference suppression in full-duplex MIMO relays," in *Proc. Conf. Rec. 44th Asilomar Conf. Signals, Syst. Comput.*, Nov. 2010, pp. 658–662.

[19] T. Riihonen, S. Werner, and R. Wichman, "Residual self-interference in full-duplex MIMO relays after null-space projection and cancellation," in *Proc. Conf. Rec. 44th Asilomar Conf. Signals, Syst. Comput.*, Nov. 2010, pp. 653–657.

IEEE *Access*

B. Li *et al.*: Self-Interference Cancellation and Channel Estimation in Multicarrier-Division Duplex Systems With Hybrid Beamforming

[20] E. Everett, C. Shepard, L. Zhong, and A. Sabharwal, "SoftNull: Many-antenna full-duplex wireless via digital beamforming," *IEEE Trans. Wireless Commun.*, vol. 15, no. 12, pp. 8077–8092, Dec. 2016.

[21] X. Liu, Z. Xiao, L. Bai, J. Choi, P. Xia, and X.-G. Xia, "Beamforming based full-duplex for millimeter-wave communication," *Sensors*, vol. 16, no. 7, p. 1130, Jul. 2016.

[22] S. Huberman and T. Le-Ngoc, "MIMO full-duplex precoding: A joint beamforming and self-interference cancellation structure," *IEEE Trans. Wireless Commun.*, vol. 14, no. 4, pp. 2205–2217, Apr. 2015.

[23] K. Satyanarayana, M. El-Hajjar, P.-H. Kuo, A. Mourad, and L. Hanzo, "Hybrid beamforming design for full-duplex millimeter wave communication," *IEEE Trans. Veh. Technol.*, vol. 68, no. 2, pp. 1394–1404, Feb. 2019.

[24] X. Guo, J. Zhang, S. Chen, X. Mu, and L. Hanzo, "Two-stage time-domain pilot contamination elimination in large-scale multiple-antenna aided and TDD based OFDM systems," *IEEE Access*, vol. 5, pp. 8629–8641, 2017.

[25] A. Yaghjian, "An overview of near-field antenna measurements," *IEEE Trans. Antennas Propag.*, vol. 34, no. 1, pp. 30–45, Jan. 1986.

[26] D. Bharadia, E. McMilin, and S. Katti, "Full duplex radios," in *Proc. ACM SIGCOMM Comput. Commun. Rev.*, 2013, vol. 43, no. 4, pp. 375–386.

[27] A. V. Oppenheim, *Discrete-Time Signal Processing*. London, U.K.: Pearson Education India, 1999.

[28] S. Gokceli, T. Levanen, T. Riihonen, M. Renfors, and M. Valkama, "Frequency-selective PAPR reduction for OFDM," *IEEE Trans. Veh. Technol.*, vol. 68, no. 6, pp. 6167–6171, Jun. 2019.

[29] A. Tang and X. Wang, "A-duplex: Medium access control for efficient coexistence between full-duplex and half-duplex communications," *IEEE Trans. Wireless Commun.*, vol. 14, no. 10, pp. 5871–5885, Oct. 2015.

[30] K. C.-J. Lin, K.-C. Hsu, and H.-Y. Wei, "Inter-client interference cancellation for full-duplex networks with half-duplex clients," *IEEE/ACM Trans. Netw.*, vol. 27, no. 5, pp. 2150–2163, Oct. 2019.

[31] A. C. Cirik and Y. Hua, "Interference management in full-duplex cellular networks," in *Full-Duplex Communications for Future Wireless Networks*. Singapore: Springer, 2020, pp. 137–163.

[32] A. F. Molisch, V. V. Ratnam, S. Han, Z. Li, S. L. H. Nguyen, L. Li, and K. Haneda, "Hybrid beamforming for massive MIMO: A survey," *IEEE Commun. Mag.*, vol. 55, no. 9, pp. 134–141, Sep. 2017.

[33] J. Hoydis, S. T. Brink, and M. Debbah, "Massive MIMO in the UL/DL of cellular networks: How many antennas do we need?" *IEEE J. Sel. Areas Commun.*, vol. 31, no. 2, pp. 160–171, Feb. 2013.

[34] K. Guo, Y. Guo, G. Fodor, and G. Ascheid, "Uplink power control with MMSE receiver in multi-cell MU-massive-MIMO systems," in *Proc. IEEE Int. Conf. Commun. (ICC)*, Jun. 2014, pp. 5184–5190.

[35] C. Rusu, R. Mendez-Rial, N. Gonzalez-Prelcic, and R. W. Heath, Jr., "Low complexity hybrid precoding strategies for millimeter wave communication systems," *IEEE Trans. Wireless Commun.*, vol. 15, no. 12, pp. 8380–8393, Dec. 2016.

[36] H. Ghauch, T. Kim, M. Bengtsson, and M. Skoglund, "Subspace estimation and decomposition for large millimeter-wave MIMO systems," *IEEE J. Sel. Topics Signal Process.*, vol. 10, no. 3, pp. 528–542, Apr. 2016.

[37] O. E. Ayach, S. Rajagopal, S. Abu-Surra, Z. Pi, and R. W. Heath, Jr., "Spatially sparse precoding in millimeter wave MIMO systems," *IEEE Trans. Wireless Commun.*, vol. 13, no. 3, pp. 1499–1513, Mar. 2014.

[38] V. N. Ha, D. H. N. Nguyen, and J.-F. Frigon, "Subchannel allocation and hybrid precoding in millimeter-wave OFDMA systems," *IEEE Trans. Wireless Commun.*, vol. 17, no. 9, pp. 5900–5914, Sep. 2018.

[39] J. P. Gonzalez-Coma, J. Rodriguez-Fernandez, N. Gonzalez-Prelcic, L. Castedo, and R. W. Heath, Jr., "Channel estimation and hybrid precoding for frequency selective multiuser mmWave MIMO systems," *IEEE J. Sel. Topics Signal Process.*, vol. 12, no. 2, pp. 353–367, May 2018.

[40] F. Sohrabi and W. Yu, "Hybrid digital and analog beamforming design for large-scale antenna arrays," *IEEE J. Sel. Topics Signal Process.*, vol. 10, no. 3, pp. 501–513, Apr. 2016.

[41] M. Wu, C. Dick, J. R. Cavallaro, and C. Studer, "High-throughput data detection for massive MU-MIMO-OFDM using coordinate descent," *IEEE Trans. Circuits Syst. I, Reg. Papers*, vol. 63, no. 12, pp. 2357–2367, Dec. 2016.

[42] H. Wei, D. Wang, J. Wang, and X. You, "TDD reciprocity calibration for multi-user massive MIMO systems with iterative coordinate descent," *Sci. China Inf. Sci.*, vol. 59, no. 10, Oct. 2016, Art. no. 102306.

[43] Z. Pi, "Optimal transmitter beamforming with per-antenna power constraints," in *Proc. IEEE Int. Conf. Commun. (ICC)*, Jun. 2012, pp. 3779–3784.

[44] S. J. Wright, "Coordinate descent algorithms," *Math. Program.*, vol. 151, no. 1, pp. 3–34, Jun. 2015.

[45] E. Telatar, "Capacity of multi-antenna Gaussian channels," *Eur. Trans. Telecommun.*, vol. 10, no. 6, pp. 585–595, Nov. 1999.

[46] M. Biguesh and A. B. Gershman, "Training-based MIMO channel estimation: A study of estimator tradeoffs and optimal training signals," *IEEE Trans. Signal Process.*, vol. 54, no. 3, pp. 884–893, Mar. 2006.

[47] Y. G. Li, J. H. Winters, and N. R. Sollenberger, "MIMO-OFDM for wireless communications: Signal detection with enhanced channel estimation," *IEEE Trans. Commun.*, vol. 50, no. 9, pp. 1471–1477, Sep. 2002.

[48] C. Shin, R. W. Heath, Jr., and E. J. Powers, "Blind channel estimation for MIMO-OFDM systems," *IEEE Trans. Veh. Technol.*, vol. 56, no. 2, pp. 670–685, Mar. 2007.

[49] J. Yue, K. Jin Kim, J. D. Gibson, and R. A. Iltis, "Channel estimation and data detection for MIMO-OFDM systems," in *Proc. GLOBECOM. IEEE Global Telecommun. Conf.*, vol. 2, Dec. 2003, pp. 581–585.

[50] Y. Li, "Simplified channel estimation for OFDM systems with multiple transmit antennas," *IEEE Trans. Wireless Commun.*, vol. 1, no. 1, pp. 67–75, Jan. 2002.

[51] *Evolved Universal Terrestrial Radio Access (E-UTRA); Base Station (BS) Radio Transmission and Reception*, document TS 36.104 version 14.3.0 release 14, 3GPP, ETSI Online, Mar. 2017.

[52] A. Sahai, G. Patel, and A. Sabharwal, "Pushing the limits of full-duplex: Design and real-time implementation," 2011, *arXiv:1107.0607*. [Online]. Available: http://arxiv.org/abs/1107.0607

[53] K. E. Kolodziej, J. G. Mcmichael, and B. T. Perry, "Multitap RF canceller for in-band full-duplex wireless communications," *IEEE Trans. Wireless Commun.*, vol. 15, no. 6, pp. 4321–4334, Jun. 2016.

[54] J.-H. Lee, "Self-interference cancelation using phase rotation in full-duplex wireless," *IEEE Trans. Veh. Technol.*, vol. 62, no. 9, pp. 4421–4429, Nov. 2013.

[55] M. A. Khojastepour, K. Sundaresan, S. Rangarajan, X. Zhang, and S. Barghi, "The case for antenna cancellation for scalable full-duplex wireless communications," in *Proc. 10th ACM Workshop Hot Topics Netw. (HotNets)*, 2011, p. 17.

[56] *136 213 v11. 3.0*, document TS 36.213 version 11.3. 0 release 11), 3GPP, LTE, vol. 178, Jul. 2013.

BOHAN LI (Member, IEEE) received the M.Sc. degree from the Beijing University of Posts and Telecommunications, in 2018. He is currently pursuing the Ph.D. degree with the Next Generation Wireless Research Group, School of Electronics and Computer Science, University of Southampton. His research interests include full-duplex systems, multicarrier communications, massive MIMO, and millimeter wave communications.

LIE-LIANG YANG (Fellow, IEEE) received the B.Eng. degree in communications engineering from Shanghai Tiedao University, Shanghai, China, in 1988, and the M.Eng. and Ph.D. degrees in communications and electronics from Northern (Beijing) Jiaotong University, Beijing, China, in 1991 and 1997, respectively. From June 1997 to December 1997, he was a Visiting Scientist with the Institute of Radio Engineering and Electronics, Academy of Sciences of the Czech Republic. Since December 1997, he has been with the University of Southampton, U.K., where he is the Professor of wireless communications with the School of Electronics and Computer Science. He has research interest in wireless communications, wireless networks and signal processing for wireless communications, as well as molecular communications and nano-networks. He has published over 390 research papers in journals and conference proceedings, authored/coauthored three books, and also published several book chapters. He is a Fellow of the IET and was a Distinguished Lecturer of the IEEE VTS. He served as an Associate Editor to the IEEE TRANSACTIONS ON VEHICULAR TECHNOLOGY and *Journal of Communications and Networks* (JCN), and is currently an Associate Editor to IEEE ACCESS and a Subject Editor to *Electronics Letters*.

ROBERT G. MAUNDER (Senior Member, IEEE) has studied with the School of Electronics and Computer Science, University of Southampton, UK, since October 2000. He received the B.Eng. degree in electronic engineering, in July 2003, and the Ph.D. degree in telecommunications, in December 2007. He began a lectureship, in November 2007, and was promoted to Associate Professor, in March 2013 and to Professor, in August 2017. He was awarded Chartered Engineer status of the IET, in November 2013, and Fellow status of the IET, in January 2017. His research interests include joint source/channel coding and the holistic design of algorithms and hardware implementations for wireless communications. He has published a number of IEEE articles in these areas. He is the founder and CTO of AccelerComm Ltd, which is commercializing his research as soft-IP.

SONGLIN SUN (Senior Member, IEEE) received the B.S. degree in radio technology and the M.S. degree in signal and information processing from the Shandong University of Technology, in June 1997 and January 2000, respectively, and the Ph.D. degree in communication and information system from the Beijing University of Posts and Telecommunications, in September 2003. He is currently a Professor with the School of Information and Communication Engineering, Beijing University of Posts and Telecommunications. His research interests include signal processing in wireless communication, video code, and multimedia transmission.

• • •